https://doi.org/10.5194/egusphere-2026-7272
Preprint. Discussion started: 25 November 2026
© Author(s) 2026. CC BY 4.0 License.

Circulation and interbasin exchange at mid-depth in the Nordic Seas from Argo floats

Erika Giorgi[1], Kjetil Våge[1], Stefanie Semper[1], Anna-Marie Strehl[1], Ailin Brakstad[1], and Ilker Fer[1]
[1]Geophysical Institute, University of Bergen, and Bjerknes Centre for Climate Research, Bergen, Norway
Correspondence: Erika Giorgi (Erika.Giorgi@uib.no)

Abstract. Dense waters from the Nordic Seas form a critical contribution to the lower limb of the Atlantic Meridional Overturning Circulation. The pathways from their source regions north of the Greenland-Scotland Ridge, however, are still not well-defined. Using 25 years of Argo float trajectories at approximately $1000\,\mathrm{m}$ depth, we map the mean mid-depth circulation and interbasin exchange of the Nordic Seas. The circulation is cyclonic, with strong flow along boundary currents, gyre rims, and steep bathymetry, while the flow in the basin interiors is generally weaker and more variable in direction. Strong cyclonic flow in the warm and saline eastern basins is well-connected, while the exchange with the colder and fresher western basins is limited. Approximately $60\,\%$ of floats remain in their deployment basin, moving cyclonically around deep isobaths, while the remainder disperse through the Nordic Seas. Some floats from the Greenland Sea are transported southward along the East Greenland Current, but most remain within the basin circulation and do not reach Denmark Strait. Southward flow along the Mohn Ridge and eastward from the central Iceland Sea merges with the Norwegian Sea Gyre, while flow along shallower isobaths can feed the Faroe Bank Channel. The circulation strengthens in winter by up to $4\,\mathrm{cm\,s^{-1}}$, broadly consistent with enhanced wind forcing and wind-stress curl. These results show that mid-depth waters are strongly retained within individual basins, with boundary currents providing the principal routes for interbasin exchange across the Nordic Seas.

https://doi.org/10.5194/egusphere-2026-7272
Preprint. Discussion started: 25 November 2026
© Author(s) 2026. CC BY 4.0 License.

1 Introduction

Dense waters formed in the Nordic Seas and Arctic Ocean supply the lower limb of the Atlantic Meridional Overturning Circulation (AMOC), a critical component of the global climate system that transports warm and saline Atlantic Water northward at the surface and returns deeper, denser waters equatorward (Kuhlbrodt et al., 2007; Chafik et al., 2019; Tsubouchi et al., 2021; Lozier, 2023). These dense waters are formed along the boundary current system and in the interior basins of the Nordic Seas and Arctic Ocean (Mauritzen, 1996; Huang et al., 2020; Brakstad et al., 2023). However, the exchanges between the basins of the Nordic Seas and the mid-depth pathways linking dense-water formation regions to the boundary currents remain poorly constrained, limiting our understanding of how waters formed in the basin interiors are redistributed. Here, we focus on the mid-depth circulation of the Nordic Seas, including the exchange between basins and the pathways upstream of the Greenland-Scotland Ridge.

Warm and saline Atlantic Water enters the Nordic Seas via two main branches across the Iceland-Faroe-Shetland Ridge and a smaller contribution to the west of Iceland (Fig. 1). The Norwegian Atlantic Slope Current (NwASC) is relatively shallow, flowing northward along the Norwegian slope, while the Norwegian Atlantic Front Current (NwAFC) flows northward as a baroclinic frontal jet along the Mohn and Knipovich Ridges (Poulain et al., 1996; Orvik and Niiler, 2002). The NwASC and the NwAFC merge into the surface-intensified West Spitsbergen Current (WSC) near Fram Strait where approximately half of the Atlantic Water enters the Arctic Ocean and the rest recirculates across the strait and joins the East Greenland Current (EGC) flowing along the western boundary (Håvik et al., 2017; Dundas and Fer, 2026). Two branches split off from the EGC into the interior: the Jan Mayen Current in the Greenland Sea (Bourke et al., 1992; Pellichero et al., 2023), and the East Icelandic Current farther south (Macrander et al., 2014; Casanova-Masjoan et al., 2020). In addition to surface waters influenced by freshwater and sea-ice transport, these branches carry subsurface waters that can recirculate within the interior basins.

The inflowing Atlantic Water is transformed through air-sea interaction and mixing processes into colder, denser Atlantic-origin waters along the boundary current and within the interior basins (Isachsen et al., 2007; Bosse et al., 2018; Huang et al., 2023; Evans et al., 2023). Dense waters are also formed in the interior basins of the western Nordic Seas, known as Arctic-origin waters, through open-ocean convection (Swift et al., 1980; Våge et al., 2015; Huang et al., 2020). The densest waters form in the Greenland Sea, where a cyclonic gyre and strong atmospheric forcing help precondition the water column for deep wintertime convection (Killworth, 1983; Marshall and Schott, 1999; Strehl et al., 2024). Both the Atlantic- and Arctic-origin waters formed at present are situated at water depths that allow them to overflow past the Greenland-Scotland Ridge. The main exit pathways are through Denmark Strait (sill depth of $650\,\mathrm{m}$) and the Faroe Bank Channel (sill depth of $840\,\mathrm{m}$). Water masses residing below these depths cannot readily cross into the North Atlantic and are largely confined to the Nordic Seas basins. Although the principal overflow branches and their downstream pathways are relatively well established, the upstream routes connecting dense-water formation regions to these branches remain uncertain.

https://doi.org/10.5194/egusphere-2026-7272
Preprint. Discussion started: 25 November 2026
© Author(s) 2026. CC BY 4.0 License.

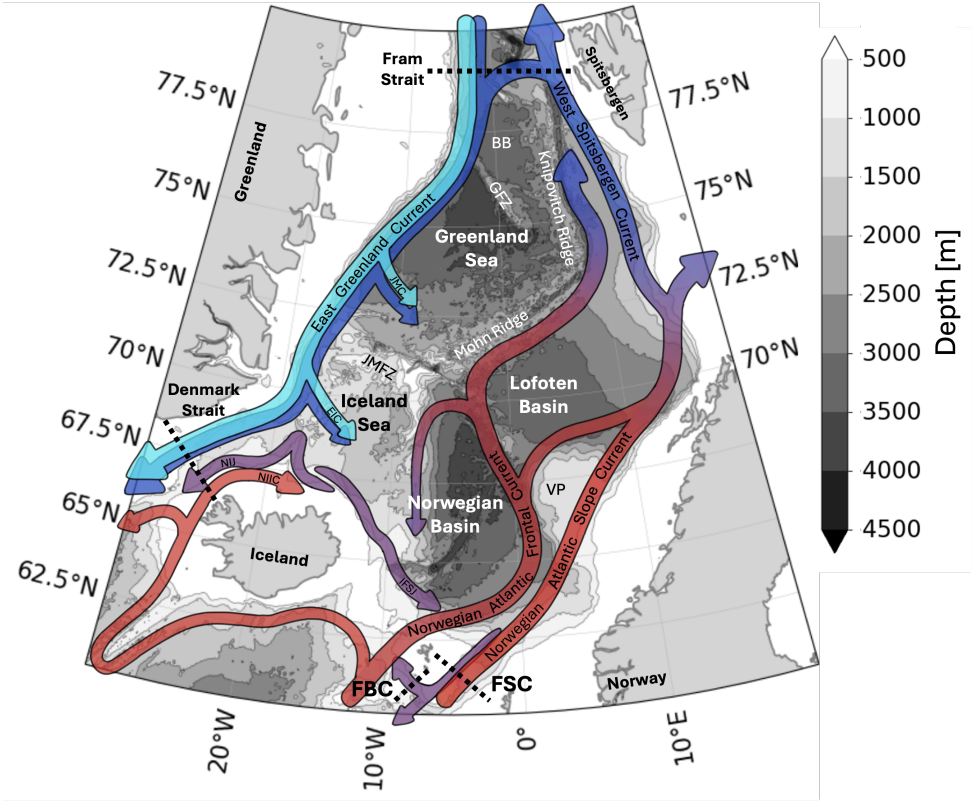

Figure 1. Schematic circulation in the Nordic Seas. Red arrows indicate the surface inflow of warm, saline Atlantic Water, with progressive cooling and densification represented by increasingly dark blue colours. Light blue arrows represent surface Polar Water. Purple arrows indicate deep dense-water pathways. The acronyms are: FBC = Faroe Bank Channel; FSC = Faroe Shetland Channel; NIIC = North Icelandic Irminger Current; JMC = Jan Mayen Current; EIC = East Icelandic Current; IFSJ = Iceland-Faroe Slope Jet; NIJ = North Icelandic Jet; JMFZ = Jan Mayen Fracture Zone; VP = Vøring Plateau, BB = Boreas Basin. The bathymetry is from GEBCO (Amante and Eakins, 2009).

At subsurface and mid-depth, the EGC transports both Atlantic- and Arctic-origin waters southward along the East Greenland slope (Jeansson et al., 2008; Håvik et al., 2019). Meanwhile, the North Icelandic Jet (NIJ), a mid-depth intensified current north-east of Iceland, transports water masses originating in the Greenland Sea, partly fed by pathways across the Jan Mayen Ridge and along an outer core of the EGC (Våge et al., 2011; Semper et al., 2019; Brakstad et al., 2023; Moe et al., 2025). Flow from the Iceland Sea also extends into the Norwegian Basin via the bottom-intensified Iceland Faroe Slope Jet (IFSJ, Semper et al., 2020). Farther downstream, the Faroe-Shetland Channel Jet carries dense water along the eastern flank of the Faroe-Shetland Channel, opposing the general cyclonic circulation of the Nordic Seas (Chafik et al., 2020, 2023). Much of this water supplying the overflows originates in the interior Greenland Sea and reaches the eastern Nordic Seas either through the Iceland Sea or by crossing the Mohn Ridge towards the south (Bringedal et al., 2018). Together, these mid-depth pathways ultimately feed the two main overflow branches at Denmark Strait and the Faroe Bank Channel. While previous studies estab-

https://doi.org/10.5194/egusphere-2026-7272
Preprint. Discussion started: 25 November 2026
© Author(s) 2026. CC BY 4.0 License.

lish several important pathway segments, the connectivity between them remains uncertain. In particular, it is not clear how consistently waters are exchanged between the basins, how much of the transport occurs within boundary currents versus the basin interiors, or how these connections vary with season.

Mid-depth circulation in the Nordic Seas is closely aligned to the bathymetry, with the flow approximately following f/H contours, where f is the Coriolis parameter and H is the water depth (LaCasce, 2000; Nøst and Isachsen, 2003). Given the strong barotropic component of the circulation, the mid-depth pathways are relevant for transport of overflow water. These pathways are also constrained by the Arctic Front, which separates the colder, fresher western basins from the warmer, more saline eastern basins The associated tilted isopycnals inhibit zonal exchange and support a northward flow near the surface and a southward flow at depth along the Mohn Ridge (Swift and Aagaard, 1981; Rossby et al., 2009; Huang et al., 2020). Experiments using Lagrangian drifters have corroborated this topographic steering both at the surface and at depth, together with faster flow during winter (Poulain et al., 1996; Jakobsen et al., 2003; Voet et al., 2010). Thus, while the Arctic Front and the underlying bathymetry determine the background circulation, its strength and variability can be modulated by atmospheric forcing.

The background circulation of the Nordic Seas is strongly influenced by the cyclonic wind stress curl, which is modulated by the North Atlantic Oscillation (NAO, Jakobsen et al., 2003). Stronger winter winds produce a seasonal barotropic response that affects the mid-depth circulation (Kolstad, 2008; Serra et al., 2010; Voet et al., 2010). The resulting increase in current speed can enhance baroclinic instability and eddy shedding, particularly along steep bathymetric features, thereby promoting exchange between boundary currents and the basin interiors (Spall, 2004; Spall et al., 2021; Johnston et al., 2025). Seasonal variations in wind forcing may therefore alter both the strength and connectivity of pathways throughout the water column. Lagrangian observations are well suited to identifying the connectivity and variability of these pathways. Here, we use 25 years of Argo data to characterize the mid-depth circulation of the Nordic Seas and to identify the pathways and interbasin exchanges connecting dense-water formation regions, boundary currents, and basin interiors.

2 Data and Methods

2.1 Argo floats, data selection, and geographical distribution

Argo floats are autonomous profiling instruments that provide quasi-Lagrangian observations of temperature, salinity, and ocean currents throughout the upper and mid-ocean (Roemmich et al., 2019). In standard mode, a float drifts at a prescribed parking depth, typically near $1000\,\mathrm{m}$, for approximately nine days before profiling to about $2000\,\mathrm{m}$ and returning to the surface for a total ten-day cycle (Wong et al., 2020). During ascent, the float measures hydrographic properties and transmits its profile and position data via satellite before beginning the next cycle. Improvements in battery technology and satellite communication since the early 2010s have extended float lifetimes and reduced surface transmission times, improving the spatial and temporal

https://doi.org/10.5194/egusphere-2026-7272
Preprint. Discussion started: 25 November 2026
© Author(s) 2026. CC BY 4.0 License.

coverage. More information on float lifetimes is given in Appendix A.

The Argo data are initially quality-controlled by automated checks of profile anomalies, and made available as real-time data after twenty-four hours. These data can be further quality-controlled through objective analysis by experts, assigning various flags to the data if there are issues with the measurements, known as delayed-mode data, which may take several months to process (Wong et al., 2020, 2025). We used both Argo delayed-mode (when available) and real-time data from April 2001 to September 2026, comprising a total of 314 floats in the Nordic Seas. We quality-controlled the data by excluding float profiles with poor position flags and trajectories containing more than five consecutive linearly interpolated surfacing positions, which typically indicate under-ice drift or unreliable positioning.

We retained only float cycles with prescribed parking depths between 1000 and 1500 m, hereafter referred to as mid-depth. This depth range samples dense and intermediate waters that can exchange between the Nordic Sea basins and may contribute to overflow pathways upstream of the Greenland-Scotland Ridge, especially due to the barotropic nature of the circulation. Following the definitions in the literature (Rudels et al., 2005; Brakstad et al., 2023), most of the waters at mid-depth here are characterized as Intermediate Waters, which can more readily supply the overflows compared to the denser waters that generally reside at greater depths (as detailed in Appendix B).

We defined the four Nordic Sea basins using boundaries drawn along the crests of submarine ridges and other shallow topographic barriers (Fig. 2a). Bathymetry along these boundaries was obtained from the GEBCO 2026 global grid at 15-arcsecond resolution. Float deployment locations were assigned to basins by their initial positions. The first mid-depth drift position may differ slightly from the deployment location, since some floats do not begin drifting at their prescribed parking depth.

2.2 Velocity estimates

Mid-depth velocities were estimated from the displacement between successive surfacing positions divided by the time elapsed between them. Each velocity estimate was assigned to the midpoint between the two surfacing locations. We excluded estimates separated by more than twelve days, allowing a two-day tolerance around the nominal full ten-day Argo cycle. Meandering of the float trajectory around topographic features increases the true distance travelled and therefore this method leads to an underestimation of the velocity.

To quantify interbasin exchange, we defined a 20 km buffer zone around each basin boundary, slightly more than double the mean Rossby radius in the Nordic Seas (Nurser and Bacon, 2014). A crossing was counted when a float trajectory transitioned from one basin to another beyond the buffer zone. The first and last positions outside the buffer were taken as the start and end points of the crossing, and the corresponding distance and time difference were used to estimate crossing velocity. The buffer zone was introduced to account for floats crossing the basin boundary several times back and forth, for example when trapped

https://doi.org/10.5194/egusphere-2026-7272
Preprint. Discussion started: 25 November 2026
© Author(s) 2026. CC BY 4.0 License.

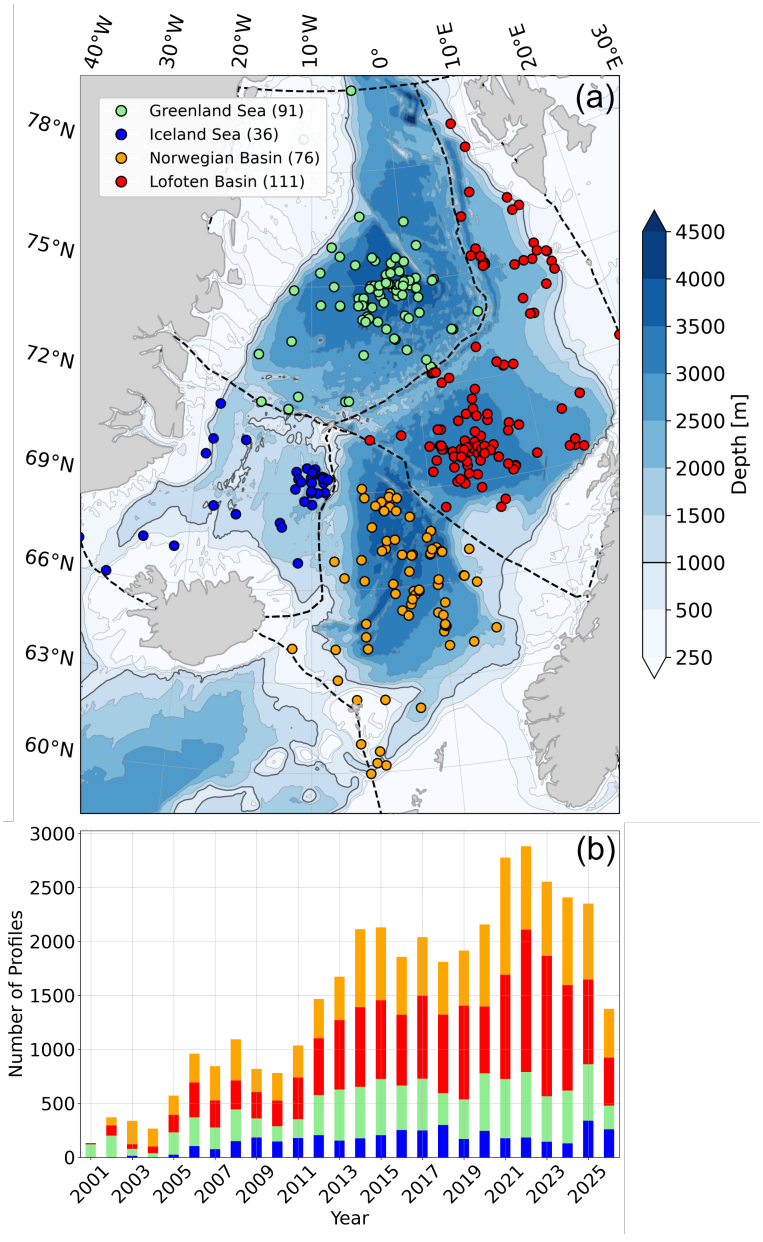

Figure 2. (a) Initial positions of Argo floats, with the total number shown in parentheses for each basin. The dashed black lines show the basin boundaries. The gray lines are the 250, 500, 1000, 1500, 2000, 2500, 3000, 3500, 4000 and 4500 m isobaths, with the 1000 m isobath drawn with a thicker line. (b) Stacked histogram of the total number of profiles taken in each basin by year. The colours correspond to the legend in panel (a).

https://doi.org/10.5194/egusphere-2026-7272
Preprint. Discussion started: 25 November 2026
© Author(s) 2026. CC BY 4.0 License.

in sub-mesoscale eddies.

The intersection between a float trajectory and boundary separating two basins is used to construct vertical sections of crossing position and velocity, gridding the velocities with Laplacian-spline interpolation (Pickart and Smethie, 1998) at a horizontal resolution of $5\,\mathrm{km}$. Because crossing velocities are estimated from the straight-line displacement between the relevant surfacing positions between basins, they should be regarded as conservative estimates. The method may also introduce errors in the assigned crossing location when the trajectory is projected onto the transect, such that some crossings may appear to lie below the bathymetry.

2.3 Anisotropic gridding

To construct a time-mean velocity field, the velocity estimates were interpolated onto a regular grid using an anisotropic distance metric. This metric accounts for the tendency of the circulation to follow isobaths: data located along similar bathymetric contours are therefore considered more representative of one another than data at the same horizontal distance but on substantially different isobaths (Nøst and Isachsen, 2003; Voet et al., 2010). Consequently, the interpolation primarily uses information along isobaths, while velocity data located across strong bathymetric gradients are assigned a larger effective distance and are less likely to contribute to the velocity estimate.

The velocity estimates, located at the midpoint between successive float positions, were mapped onto a grid with a resolution of $1/3°$ in longitude and $1/8°$ in latitude. For each velocity position and grid point, we calculated an effective distance, r, that combines their horizontal separation with their difference in bottom depth:

$$r^2 = |\mathbf{x}_a - \mathbf{x}_b|^2 + \left| 3\lambda \frac{H_a - H_b}{H_a + H_b} \right|^2 . \tag{1}$$

Here, $\mathbf{x}_a$ and $\mathbf{x}_b$ denote the positions of the grid point and the velocity estimate, respectively, while H_a and H_b are the corresponding bottom depths obtained from the GEBCO bathymetry product. The first term represents the geographical distance between the data and the grid point; the second increases the effective distance when the two locations have different bottom depths. When the bottom depths are equal, the effective distance equals the geographical distance. If one bottom depth is twice the other, the bathymetric term contributes λ^2 to r^2. Generally, when the bottom depths differ, the effective distance is larger, even if the two locations are geographically close. Thus, velocity estimates located across isobaths may be excluded from the interpolation, whereas estimates that are farther away horizontally but lie along similar isobaths may still be included.

The topographic scaling parameter λ was set to $100\,\mathrm{km}$ following Voet et al. (2010). We retained data satisfying $r \leq 50\,\mathrm{km}$, where the threshold refers to the effective distance r^2 rather than the geographical distance. The mean velocity at each grid

https://doi.org/10.5194/egusphere-2026-7272
Preprint. Discussion started: 25 November 2026
© Author(s) 2026. CC BY 4.0 License.

point was then calculated from the data within this effective radius.

The number of observations contributing to each grid point is highest in the basin interiors, particularly in the deepest parts of the Greenland Sea and the Lofoten Basin, whereas the boundary regions are more sparsely sampled (Fig. 3). This pattern reflects both the distribution of float trajectories and the anisotropic distance criterion, which limits the use of observations across strong bathymetric gradients. The northwestern Iceland Sea has limited coverage because parts of this region are shallower than the float parking depths considered here.

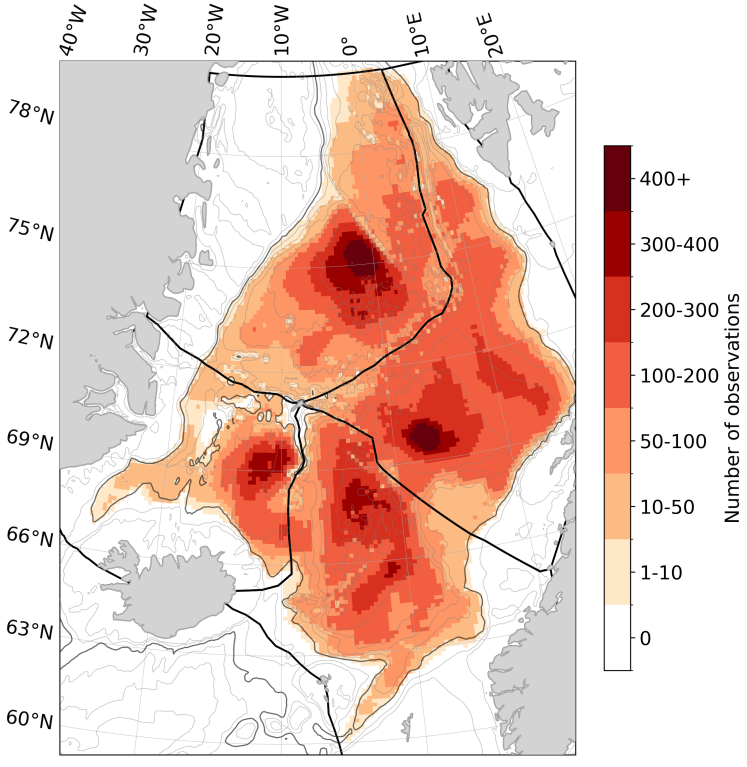

Figure 3. Map showing the number of velocity estimates within a 50 km effective radius of each grid point used for the anisotropic gridding. The isobaths are the same as for Figure 2. The black lines are the boundaries separating the basins.

https://doi.org/10.5194/egusphere-2026-7272
Preprint. Discussion started: 25 November 2026
© Author(s) 2026. CC BY 4.0 License.

2.4 Topostrophy

As the bathymetry largely steers the flow of the Nordic Seas, we quantify this alignment with the topostrophy parameter T (Killworth, 1992; Holloway et al., 2007). Topostrophy T is defined as the vertical component of the cross product between the horizontal velocity vector, v, and the horizontal gradient of the bottom depth, ∇H:

$$T = (\boldsymbol{v} \times \boldsymbol{\nabla} H)_z, \tag{2}$$

Because T depends on both the magnitude of the velocity and the bathymetric gradient, we use the normalized topostrophy,

$$\hat{T} = \frac{(\boldsymbol{v} \times \boldsymbol{\nabla} H)_z}{|\boldsymbol{v}| \cdot |\boldsymbol{\nabla} H|} \tag{3}$$

The normalized topostrophy varies between -1 and 1 and measures the orientation of the flow relative to the local bathymetry. Positive and negative values indicate cyclonic and anticyclonic flow, respectively, while larger absolute values indicate stronger alignment between the flow and the isobaths. Values approaching $+1$ or -1 therefore represent flow that is approximately parallel to the isobaths, while $\hat{T} = 0$ indicates flow directed perpendicular to the isobaths.

2.5 Reanalysis products

Argo float sampling is uneven in both space and time, particularly in the boundary-current regions (Fig.3) and during winter due to the presence of sea ice in the western basins. We therefore compare the Argo-derived velocities with the GLORYS12 reanalysis, which provides a gridded and dynamically constrained Eulerian velocity field (Lellouche et al., 2021). GLORYS12 is a global ocean reanalysis with a horizontal resolution of $1/12°$ and 50 vertical levels, assimilating Argo hydrographic profile data but not their trajectories. Monthly mean eastward and northward velocities were extracted for the Nordic Seas from January 2001 to May 2026. This comparison allows us to assess whether the main circulation features inferred from the Lagrangian float trajectories are consistent with the reanalysis and provides spatial context in regions where the Argo sampling is sparse.

We first compare the mean and seasonal velocity fields from our Argo to the GLORYS12 fields at $1000\,\mathrm{m}$. Winter and summer means were calculated from November to April and May to October, respectively, and the seasonal difference was defined as winter minus summer. We then use the GLORYS12 velocity fields at the surface and $500\,\mathrm{m}$ together with atmospheric forcing to examine the vertical coherence of the circulation and the possible barotropic influence on the mid-depth flow.

ERA5 atmospheric fields (Hersbach et al., 2020) were used to examine whether seasonal differences in the circulation are consistent with changes in wind forcing. Monthly mean fields of the instantaneous eastward and northward turbulent surface stress were used to calculate the vertical component of the wind-stress curl over the Nordic Seas:

$$(\nabla \times \boldsymbol{\tau})_z = \frac{\partial \tau_y}{\partial x} - \frac{\partial \tau_x}{\partial y}, \tag{4}$$

https://doi.org/10.5194/egusphere-2026-7272
Preprint. Discussion started: 25 November 2026
© Author(s) 2026. CC BY 4.0 License.

where τ_x and τ_y denote the eastward and northward surface-stress components, respectively. Areas with more than $15\,\%$ sea ice concentration in a grid cell were removed.

3 Mean circulation

The mean mid-depth flow is predominantly cyclonic around the Nordic Seas and within the individual basins (Figs. 4 and 5). The highest mean speeds, exceeding $10\,\mathrm{cm\,s^{-1}}$, occur along boundary currents and regions of steep bathymetry, whereas the basin interiors are characterized by weaker flow. The main features of the circulation are the cyclonic gyre in the Lofoten Basin, approximately enclosed by the $3000\,\mathrm{m}$ isobath; the Norwegian Sea Gyre, linked with southward flow along the Mohn Ridge; and strong southward flow along the northern EGC. These features are also apparent in the topostrophy field: high positive values occur along the boundary currents and steep isobaths, indicating cyclonic flow aligned with the bathymetry (Fig. 5). Topostrophy in the basin interiors is generally closer to zero, consistent with weaker flow and a less pronounced alignment with local bathymetry.

Within the Greenland Sea, the EGC is strongest south of the Boreas Basin, coinciding with high positive topostrophy values (Figs. 4 and 5). Part of the EGC turns eastward into the interior Greenland Sea along deep isobaths, particularly along the Jan Mayen Current, and returns northward along the Mohn and Knipovich Ridges, forming a broad but relatively weak ($\leq 3\,\mathrm{cm\,s^{-1}}$) pathway. In the northern the Greenland Sea, this flow merges with the EGC, both along the Greenland Fracture Zone and through the Boreas Basin (Fig. 4).

In the Iceland Sea, the EGC signal weakens towards Denmark Strait, approximately corresponding to the location of where the East Icelandic Current branches off (Fig. 4). This reduction in mean velocity along the southern portion of the EGC coincides with relatively few floats in the region (Fig. 3) and floats that are recirculated due to the shoaling bathymetry (Fig. 6), reflecting limited sampling rather than a reduction in the current itself. Higher mean velocities are present towards Denmark Strait, along with negative topostrophy values. This is consistent with the NIJ along the slope north of Iceland extending towards Denmark Strait (Fig. 5).

In the eastern Iceland Sea, a weak pathway extends from the basin interior towards the Icelandic slope, continuing eastward towards the Norwegian Basin along approximately the $1000\,\mathrm{m}$ isobath (Fig. 4). A similar pathway has been identified from RAFOS floats drifting at $700\,\mathrm{m}$ (de Jong et al., 2018) and from surface-drifter observations (Søiland et al., 2008; Semper et al., 2022). They also observe a double-gyre circulation in this region, evident from the trajectory density field here, also highlighting the limited connection between the western and eastern parts of this basin (Fig. 6).

https://doi.org/10.5194/egusphere-2026-7272
Preprint. Discussion started: 25 November 2026
© Author(s) 2026. CC BY 4.0 License.

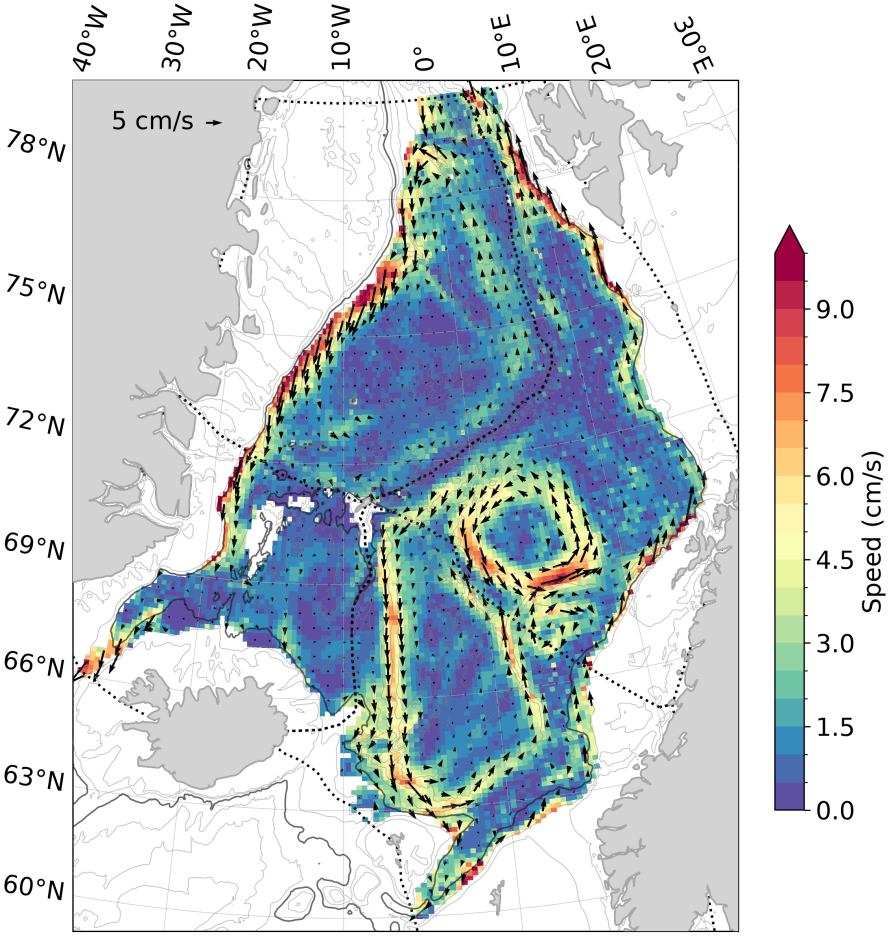

Figure 4. Mean mid-depth velocity of the Nordic Seas. Areas in white indicate missing or removed data. Only grid cells with more than three velocity estimates are included. The isobaths are the same as for Figure 2.

The flow from the Iceland Sea into the Norwegian Basin is initially distinct from the Norwegian Sea Gyre but merges with it north of the Faroe Islands (Figs. 4 and 6). Farther south, part of the flow is directed towards the Faroe-Shetland Channel, while the remainder follows deeper isobaths and recirculates within the Norwegian Basin or continues towards the Lofoten Basin. Within the Norwegian Basin, the circulation bifurcates near the western edge of the Vøring Plateau: one branch continues northward, whereas another recirculates and forms part of the Norwegian Sea Gyre. Topostrophy is predominantly positive throughout the Norwegian Basin, especially along along the gyre following steep isobaths (Fig. 5). Negative values of topostrophy are found along the shallower slope extending from the Vøring Plateau towards the Faroe Shetland Channel. The flow upstream of this channel is consistent with the Faroe-Shetland Channel Jet, which follows the eastern side of the channel and locally opposes the dominant cyclonic circulation (Søiland et al., 2008; Chafik et al., 2020).

https://doi.org/10.5194/egusphere-2026-7272
Preprint. Discussion started: 25 November 2026
© Author(s) 2026. CC BY 4.0 License.

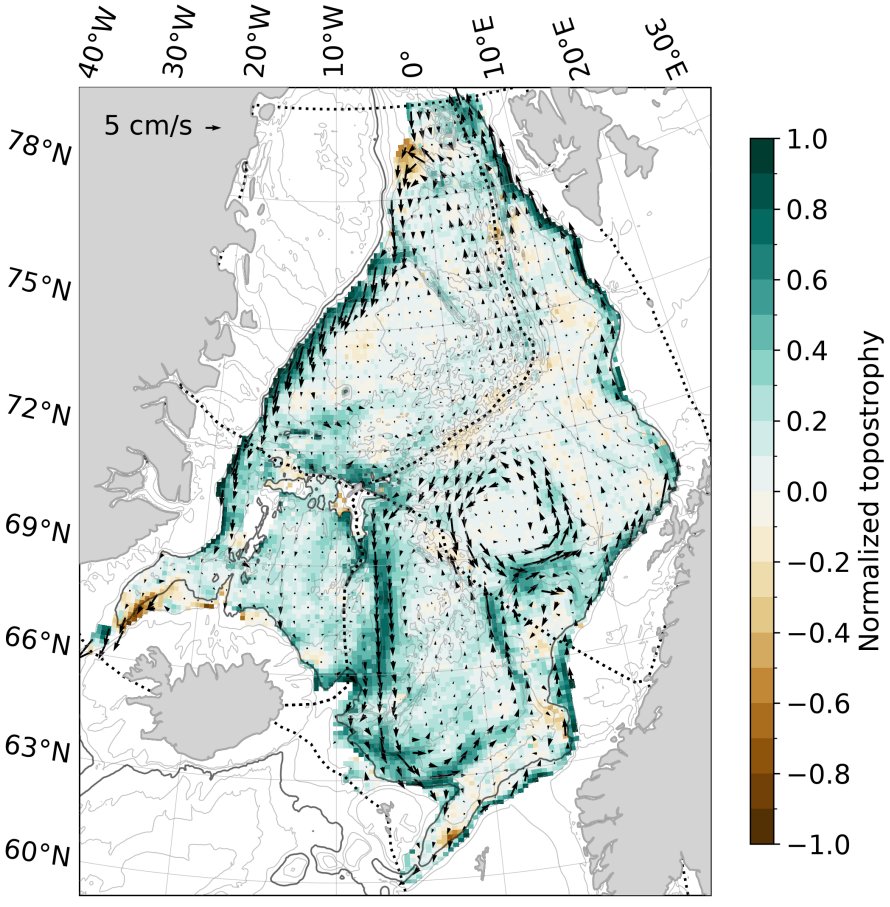

Figure 5. Mean mid-depth topostrophy of the Nordic Seas. Areas in white indicate missing or removed data. Only grid cells with more than three velocity estimates are included.The isobaths are the same as for Figure 2.

Within the Lofoten Basin, the cyclonic gyre is strongest along the southern rim and near the slope of the Vøring Plateau, where topostrophy is also enhanced (Figs. 4 and 5). Although velocities in the deep Lofoten Basin interior are low, many floats cross this region or are trapped within the Lofoten Vortex with velocities cancelling out in the long-term mean (Fig. 6). A distinct branch, flowing southward along the Mohn Ridge, turns into the interior Lofoten Basin, while another part of it continues into the Norwegian Basin. Along the eastern boundary of the Lofoten Basin, relatively high velocities occur near the slope close to the Lofoten Islands and farther north along the West Spitsbergen Current towards Svalbard, with slightly lower velocities in-between. Northward flow along the Knipovich Ridge strengthens towards Fram Strait, where it merges with the current along the continental slope before either continuing towards the Arctic Ocean or recirculating into the Greenland Sea.

https://doi.org/10.5194/egusphere-2026-7272
Preprint. Discussion started: 25 November 2026
© Author(s) 2026. CC BY 4.0 License.

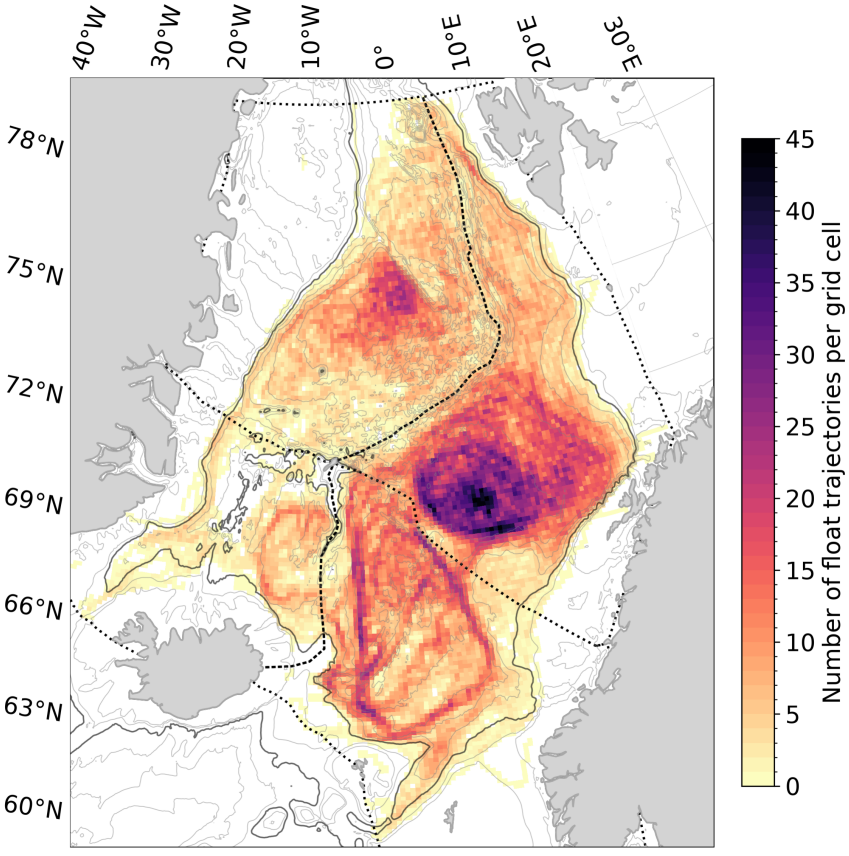

Figure 6. Heatmap of Argo float trajectory density based on all line segments connecting consecutive surfacing positions. The shading indicates the number of trajectory segments crossing each grid cell, with darker colours representing higher counts. The isobaths are the same as for Figure 2.

The trajectory density field also indicates exchange between the basin interiors and the boundary currents (Fig. 6). In the Lofoten Basin, some floats following the boundary current move into the basin interior, possibly associated with the steep bathymetry and energetic mesoscale variability in the region (Spall et al., 2021; Johnston et al., 2025). In the central Greenland Sea, several trajectories cross isobaths from the basin interior into the EGC, indicating exchange between the weaker interior circulation and the faster boundary current (Fig. 6). Baroclinic instabilities along steep bathymetry can generate eddies that more readily supply waters from the interior towards the boundary currents, as shown in an idealized model simulation of Yang and Pratt (2013). Similar exchange has been documented between the boundary current and the Greenland Sea interior between 75 and 76°N (e.g., Strass et al., 1993; Håvik et al., 2019; Brakstad et al., 2023).

https://doi.org/10.5194/egusphere-2026-7272
Preprint. Discussion started: 25 November 2026
© Author(s) 2026. CC BY 4.0 License.

4 Interbasin exchange

4.1 Float migration

Approximately 60 % of the floats remained within their deployment basin throughout their tracking period (mean lifetime of 3.5 years, see Appendix A), indicating substantial retention within the Nordic Seas basins (Fig. 7). Floats that left their deployment basin did so after a mean residence time of 1.5 years, and all such exits occurred within 6 years of deployment (Fig. A1). Retention was lowest in the Iceland Sea, where 50 % of the floats remained in the basin. Exchange with neighbouring basins increased with integration time and occurred mainly along boundary-current pathways and topographically guided routes. These pathways connect the interior basins and provide routes toward the North Atlantic and Arctic Ocean.

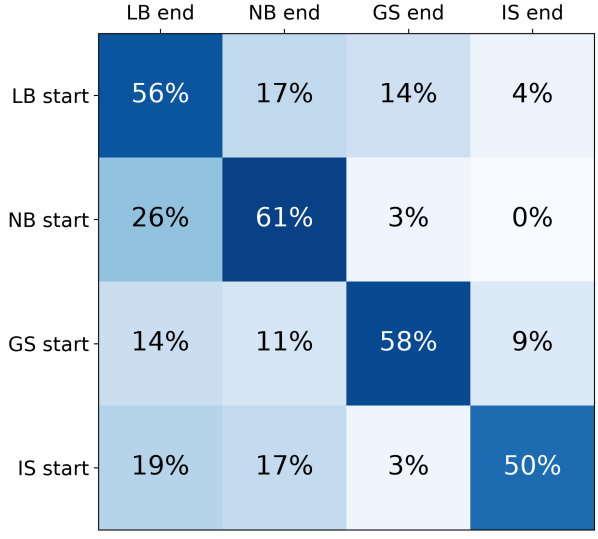

Figure 7. Heat map matrix of starting and ending locations of the floats, given as a percentage. The starting basin is shown as the y-axis, the ending basins are on the x-axis. Dark colours represent more floats remaining in the basin they were deployed in. Acronyms are LB: Lofoten Basin, NB: Norwegian Basin, GS: Greenland Sea and IS: Iceland Sea. Rows not adding up to 100 % indicate floats leaving the Nordic Seas.

The floats from the Greenland Sea were primarily deployed in the deepest part of the basin, with relatively limited movement to neighbouring basins (Figs. 8a and 7). Floats that entered the eastern basins from the Greenland Sea were largely incorporated into the circulation of the Lofoten Basin or the Norwegian Sea Gyre. The trajectories showed two distinct pathways from the Greenland Sea towards the southern Nordic Seas. A relatively small number of floats (3 out of 91) followed the EGC southward and reached Denmark Strait after two to four years; these remained distinct from floats that crossed into the interior Iceland Sea through gaps in the West Jan Mayen Ridge and subsequently followed the cyclonic circulation towards the Norwegian Basin (Fig. 8a). Among the floats entering the eastern Nordic Seas, those following shallower isobaths (near 1500 m) moved toward

https://doi.org/10.5194/egusphere-2026-7272
Preprint. Discussion started: 25 November 2026
© Author(s) 2026. CC BY 4.0 License.

the Faroe-Shetland Channel, whereas those following deeper isobaths continued northward.

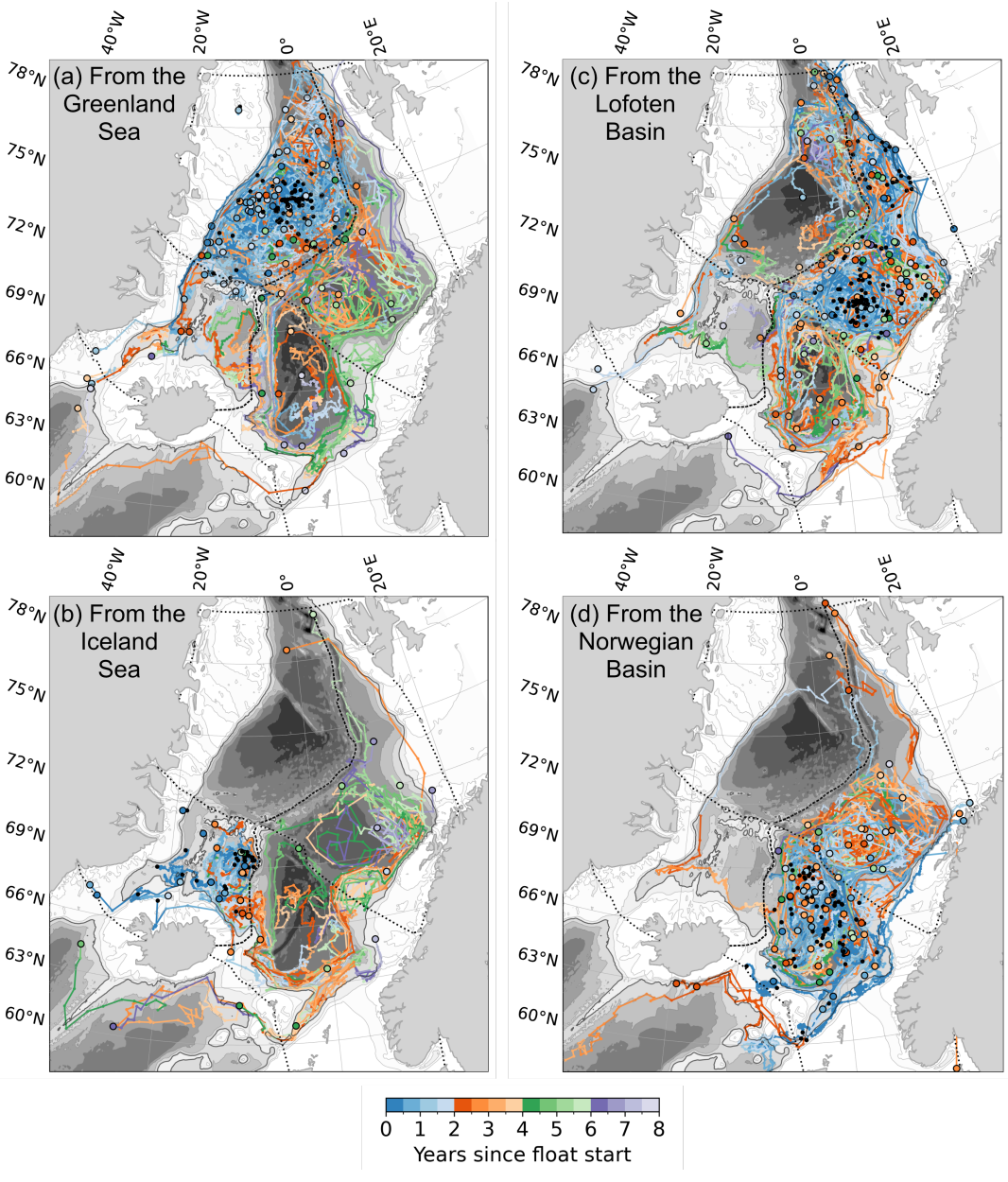

Figure 8. Trajectories of all Argo floats in the Nordic Seas with segments colored by time since float deployment. The starting (black dots) and ending (coloured circles) positions are shown and coloured by the years since the float started in the respective basins: (a) Greenland Sea, (b) Iceland Sea, (c) Lofoten Basin, and (d) Norwegian Basin. Small dots along the trajectories indicate profile positions. The isobaths are the same as for Figure 2.

https://doi.org/10.5194/egusphere-2026-7272
Preprint. Discussion started: 25 November 2026
© Author(s) 2026. CC BY 4.0 License.

The floats from the Iceland Sea were primarily deployed in the deep northeastern part of the basin, and remained there for up to six years, although half of the floats dispersed out of the Iceland Sea within two to five years (Fig. 8b). Most of the floats leaving this basin followed the boundary-current system within the Norwegian and Lofoten Basins. After reaching the Lofoten Basin, some floats entered its interior after passing the Vøring Plateau. These trajectories may reflect the tendency of floats to keep following the isobaths they were deployed on, although the energetic boundary-current region and steep topography may also have facilitated exchange between the boundary current and the basin interior. None of the floats deployed in the central Iceland Sea reached Denmark Strait, rather being deflected eastward by the topographic barriers and generally cyclonic circulation of the Nordic Seas. Only three floats passed through the Faroe Bank Channel.

Most of the Lofoten Basin floats were deployed within the deepest isobaths, remaining in this basin for up to six years (Figs. 8c and A1). Among the floats that left this basin, most moved into the Norwegian Basin, flowing around the boundary current rather than merging with the interior or exiting towards the Faroe Bank Channel. Few floats entered the Greenland Sea across the Mohn and Knipovich Ridges from the Lofoten Basin. Instead, floats that left this basin to the north either travelled into the Arctic Ocean or recirculated in Fram Strait before entering the Boreas Basin. Some floats (5 out of a total of 111) were transported southward along the EGC, with only two of these reaching Denmark Strait within two years while the rest were recirculated north of Iceland.

Floats deployed in the Norwegian Basin were largely confined to the gyres of the eastern Nordic Seas (Fig. 8d). Following deployment, around half of the floats remained within the central Norwegian Basin while the rest followed the deep isobaths connecting the Norwegian and Lofoten Basins. A subset entered the Lofoten Basin along the shelf, where the trajectories were generally deflected into the interior and subsequently recirculated within the Lofoten Gyre. Only a few floats continued beyond the eastern basins, including three pathways along the slope toward Fram Strait. One float completed a cyclonic circuit around the Nordic Seas within approximately four years, including one year of southward propagation along the EGC from the Boreas Basin towards Denmark Strait. This trajectory demonstrates the potential for longer-range connectivity, although it was not representative of the dominant pathways from the Norwegian Basin.

Overall, the float trajectories show that mid-depth motion is strongly constrained by bathymetry. Floats generally remained within their deployment basin unless they entered a boundary current. The shallow sills of the Greenland-Scotland Ridge relative to the drift of the Argo floats limited the number of instances that floats crossed the ridge, although crossings could occur while floats were at the surface or during profiling. Only floats deployed in the Greenland Sea and Lofoten Basin passed through Denmark Strait. Floats from all basins passed through the Faroe Bank Channel, but the small amount of floats implies that these trajectories should not be interpreted as a robust estimate of the relative contribution from each basin due to the float drift depth being below the sill depths of both overflow regions.

https://doi.org/10.5194/egusphere-2026-7272
Preprint. Discussion started: 25 November 2026
© Author(s) 2026. CC BY 4.0 License.

4.2 Jan Mayen to Greenland - exchange between the Greenland and Iceland Seas

The West Jan Mayen Ridge provides a bathymetrically rough boundary running westward from Jan Mayen, separating the Greenland and Iceland Seas (Fig. 9). Before the ridge reaches the Greenland slope, it opens into a sill of approximately $1700\,\mathrm{m}$ depth, which provides an easy passage for the surface-intensified EGC, but hinders deeper southward transport between the two basins. Just north of the West Jan Mayen Ridge, some floats are deflected into the Greenland Sea from the southward trajectory along the EGC before crossing the ridge into the Iceland Sea (Fig. 9a). This bathymetric configuration provides a pathway for flow along the Greenland slope, while also allowing some limited exchange between the basin interiors across the West Jan Mayen ridge.

All of the floats crossed this section from north to south, with one float crossing back into the Greenland Sea before being transported southward again across the West Jan Mayen Ridge (Fig. 9). The southward flow reached velocities of more than $10\,\mathrm{cm\,s^{-1}}$ along the EGC, with slower and more dispersed southward flow across the ridge. Most floats crossing the section originated in the central Greenland Sea, and entered the EGC just south of the Boreas Basin (Fig. 9a). Four of the floats crossing this section passed through Denmark Strait, while the rest recirculated northward near 68°N and continued eastward along the Icelandic slope. These floats joined pathways from the interior Iceland Sea near the Kolbeinsey Ridge before continuing into the Norwegian Sea, mostly along the $2000\,\mathrm{m}$ isobath.

https://doi.org/10.5194/egusphere-2026-7272
Preprint. Discussion started: 25 November 2026
© Author(s) 2026. CC BY 4.0 License.

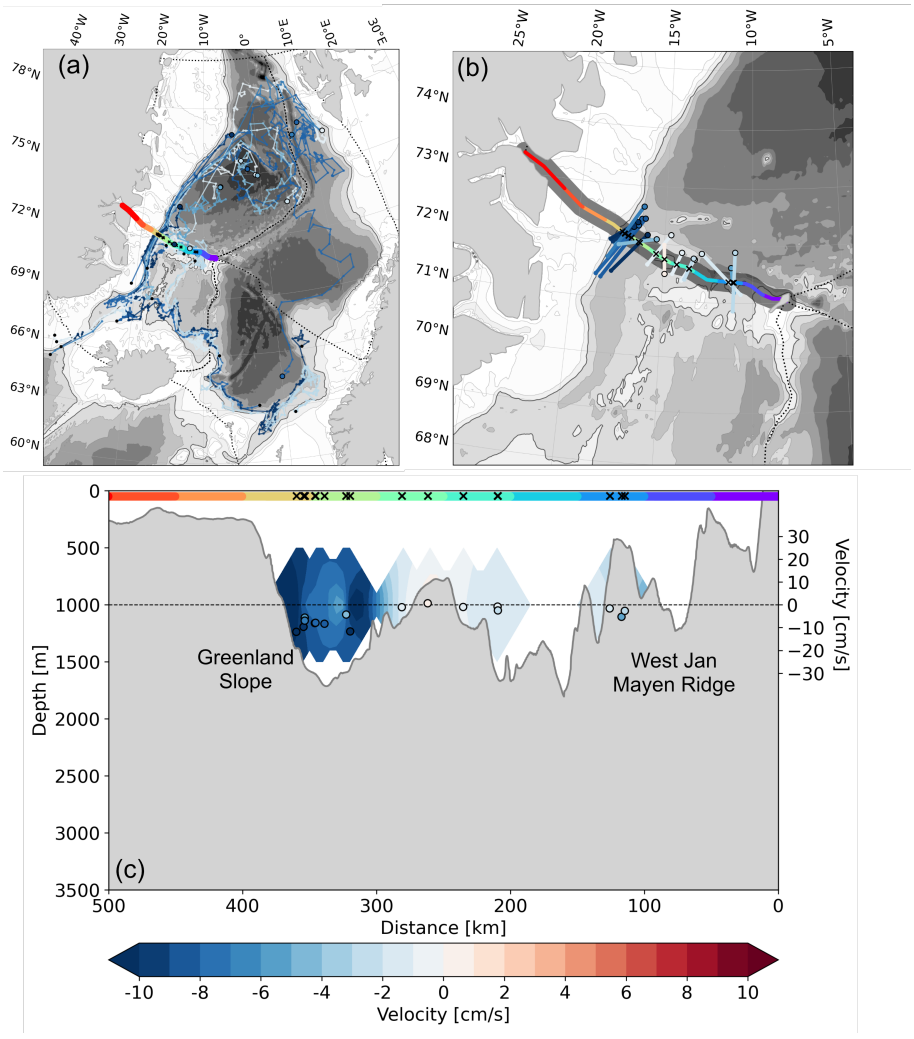

Figure 9. Exchange between the Greenland and Iceland Seas. (a) Trajectories crossing the section between Jan Mayen and Greenland, coloured by mean crossing velocity (blue: Greenland Sea to Iceland Sea; red: Iceland Sea to Greenland Sea). The coloured circles are the starting locations and the black dots show the final locations. The multi-coloured line shows distance from Jan Mayen in intervals of 50 km for all panels, with black crosses indicating individual crossing locations. (b) Enlargement of the crossing locations coloured by individual crossing velocity. (c) A vertical transect along the section, with bathymetry in grey, gridded crossing velocity as background shading and individual float crossings shown as dots, with vertical extent corresponding to the right y-axis showing velocity. The black crosses in all panels mark crossing locations. The isobaths in (a) and (b) are the same as for Figure 2.

https://doi.org/10.5194/egusphere-2026-7272
Preprint. Discussion started: 25 November 2026
© Author(s) 2026. CC BY 4.0 License.

4.3 Jan Mayen to Iceland - exchange between the Iceland Sea and Norwegian Basin

The Jan Mayen–Iceland section is used to examine exchange between the Iceland Sea and the Norwegian Basin. This section spans the Jan Mayen Ridge and its southern flank towards the Icelandic slope (Fig. 10), thereby intersecting the region where flow associated with the East Icelandic Current and IFSJ may contribute to the exchange. The ridge system is also associated with the Arctic Front, which can limit direct exchange between the western and eastern basins (Swift and Aagaard, 1981).

Most eastward-crossing floats originated in the northeastern Iceland Sea (Fig. 10a). They typically recirculated within the Iceland Sea before moving southward along the Kolbeinsey Ridge and then eastward along the Icelandic slope towards the Norwegian Basin. The eastward crossings were generally slow and spatially dispersed, with velocities below $5\,\mathrm{cm\,s^{-1}}$. A hotspot of crossings occurs between approximately 400 and $500\,\mathrm{km}$ from Jan Mayen, with most floats flowing eastward through a narrow channel, with fewer, more dispersed floats crossing further south (Fig.10b,c). After entering the eastern Nordic Seas, most of the floats remained within the Norwegian and Lofoten basins, while a minority exited through the Faroe Bank Channel.

As most of the flow in the Norwegian Basin is advected directly southward along the rim current (Fig. 4), this can limit the exchange to the west, at least at mid-depth. However, there is some indication of flow crossing the Jan Mayen Ridge at shallower depths from previous studies (Mork et al., 2014; Brakstad et al., 2023). Across the section here, only four floats crossed from the Norwegian Basin into the Iceland Sea, originating either in the central Greenland Sea or Lofoten Basin (Fig. 10a). These trajectories appear to cross the Jan Mayen Ridge at slightly shallower depths than $1000\,\mathrm{m}$, likely flowing around the southern end of the ridge through the Hlessund Trough (Fig. 10c).

The float trajectories therefore support the view that exchange between the western and eastern basins occurs mainly through narrow, topographically controlled routes rather than through direct basin-wide flow across the Arctic Front. These pathways may contribute to the downstream supply of water towards the Greenland–Scotland Ridge, although the Argo trajectories sample the mid-depth circulation and do not directly resolve overflow transport.

https://doi.org/10.5194/egusphere-2026-7272
Preprint. Discussion started: 25 November 2026
© Author(s) 2026. CC BY 4.0 License.

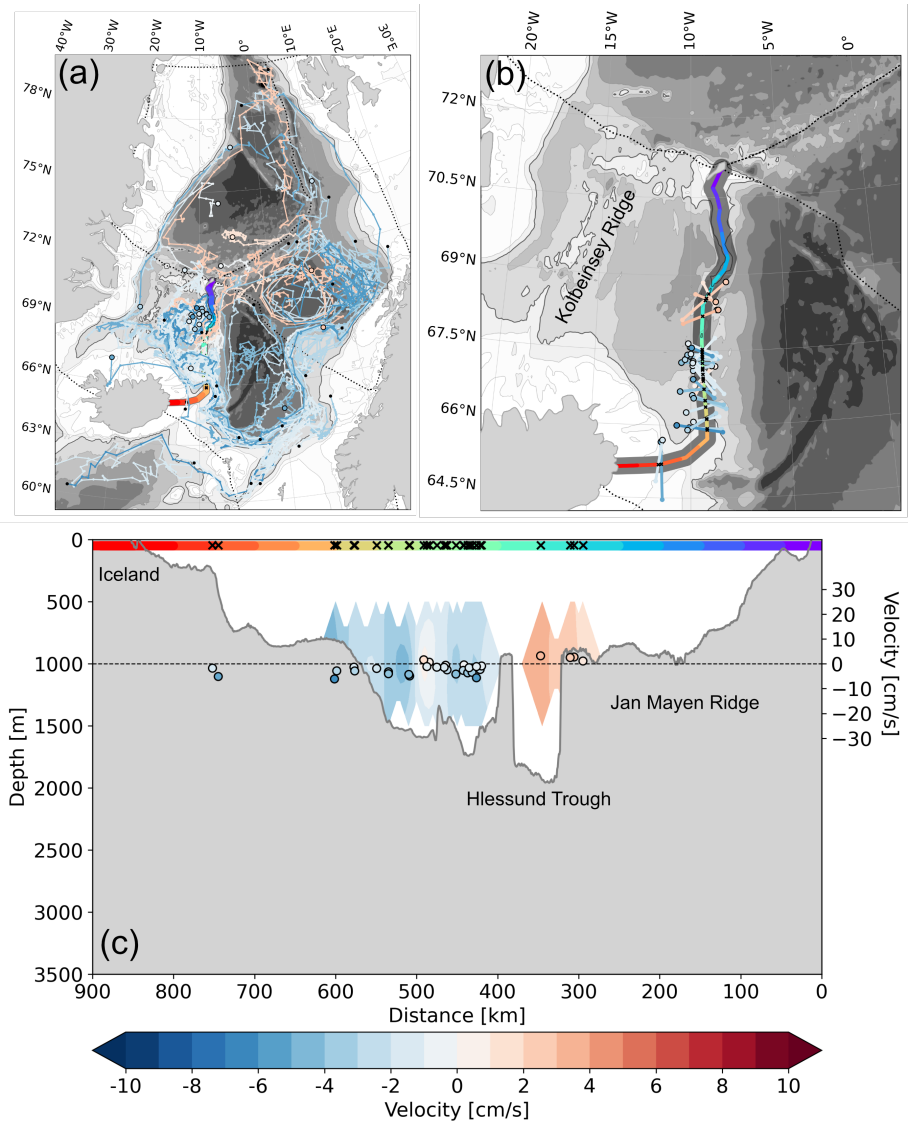

Figure 10. Exchange between the Iceland Sea and the Norwegian Basin. Panels and symbols are the same as in Figure 9. Blue trajectories and colours indicate crossings from the Iceland Sea to the Norwegian Basin, and red trajectories and colours indicate crossings in the opposite direction. The isobaths in (a) and (b) are the same as for Figure 2.

4.4 Jan Mayen to Norway - exchange between the Lofoten and Norwegian Basins

The Norwegian and Lofoten Basins are well-connected (as also seen in Figure 8c,d), with deep passages exceeding 3000 m (Fig. 11). At the eastern end of the section defined here, the shallow Vøring Plateau and Norwegian shelf limit deep exchange between the basins. The plateau is approximately 1300 m deep and connects to the shelf, where water depths are generally

https://doi.org/10.5194/egusphere-2026-7272
Preprint. Discussion started: 25 November 2026
© Author(s) 2026. CC BY 4.0 License.

less than $500\,\mathrm{m}$. Between Jan Mayen and the Vøring Plateau, the bathymetry divides the section into eastern and western deep regions. This division is reflected in the velocity structure across the section with strong southward flow (around $8\,\mathrm{cm\,s^{-1}}$) in the west and strong northward flow around the Vøring Plateau in the east corresponding to the NwASC, with anticyclonic recirculation on the Plateau itself (Fig. 11b,c).

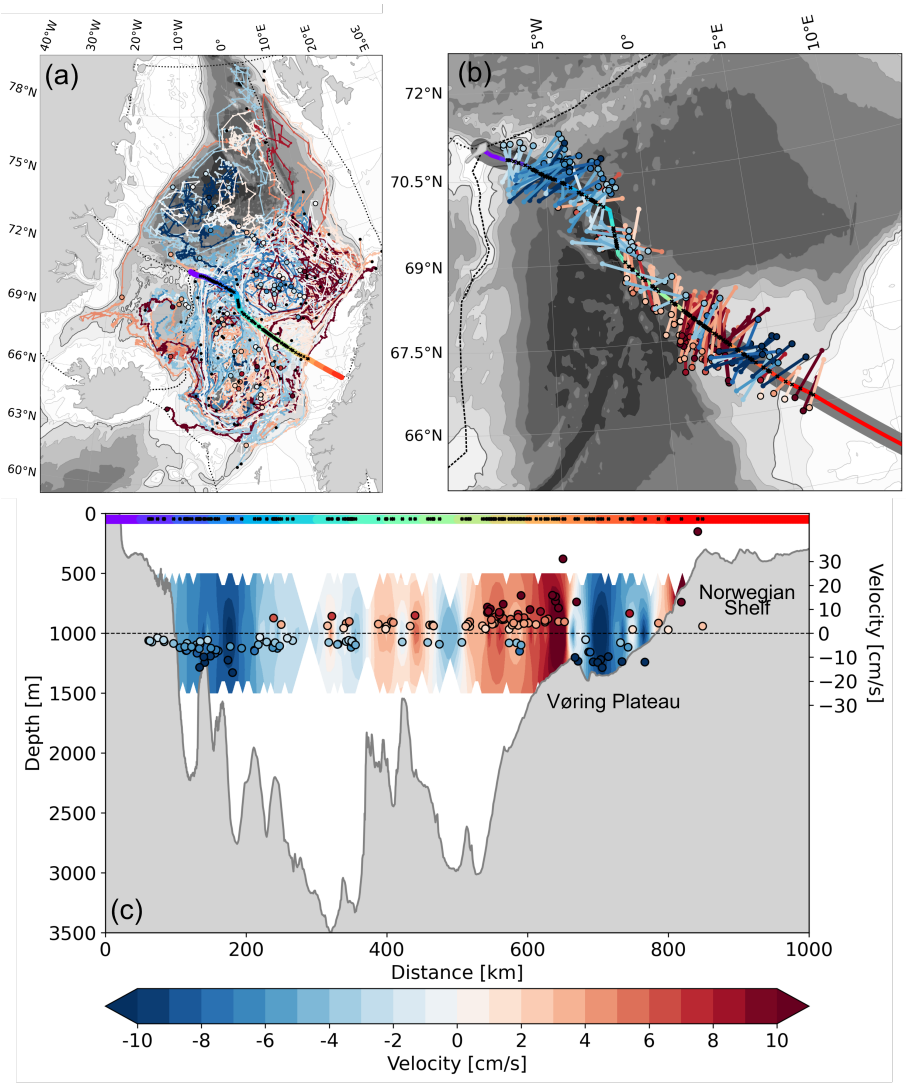

Figure 11. Exchange between the Norwegian Basin and the Lofoten Basin. Panels and symbols are the same as in Figure 9. Blue trajectories and colours indicate crossings from the Lofoten Basin to the Norwegian Basin, and red trajectories and colours indicate crossings in the opposite direction. The isobaths in (a) and (b) are the same as for Figure 2.

https://doi.org/10.5194/egusphere-2026-7272
Preprint. Discussion started: 25 November 2026
© Author(s) 2026. CC BY 4.0 License.

Most floats crossing the section originated in the Norwegian or Lofoten Basins, reflecting the strong connection between these two basins and the weaker zonal connection to the western basins (Fig. 11a). The exchange here has a predominantly cyclonic structure, with the strongest and most coherent pathways along the steep basin margins, and weaker, more dispersed crossing in-between, despite the deeper topographic gaps (Fig. 11b,c).

4.5 Jan Mayen to Fram Strait - exchange between the Greenland Sea and Lofoten Basin

From Jan Mayen towards Fram Strait, the Mohn and Knipovich Ridges, together with the Arctic Front, form a barrier between the Greenland Sea to the west and the Lofoten Basin to the east (Orvik and Niiler, 2002; Rossby et al., 2009). The float trajectories crossing this section indicate exchange in both direction, but coherent pathways are largely absent over most of the ridges (Fig.12). A hotspot of trajectories crossed from the Greenland Sea into the Lofoten Basin over the Mohn Ridge at approximately $400\,\mathrm{km}$ from Jan Mayen (Fig.12c). This pattern is consistent with the previously reported supply of mid-depth waters from the Greenland Sea across the Mohn Ridge as seen from hydrographic observations (Wang et al., 2021). In contrast, relatively few trajectories crossed the Knipovich Ridge into the Lofoten Basin.

Near the southern end of the section, the Jan Mayen Channel provides a potential pathway for deep exchange into the Lofoten Basin (Hansen and Østerhus, 2000; Pellichero et al., 2023). Only two floats originating in the Greenland Sea crossed through the Jan Mayen Channel here (Fig. 12c). The limited flow through the channel at mid-depth suggests that it was not an important pathway for the exchange sampled here. Nevertheless, flow reversals through the channel have been documented in response to changes in the density gradient between the two basins, highlighting its potential importance for dense-water exchange and as a source region for overflows into the North Atlantic (Østerhus and Gammelsrød, 1999).

The ridges are characterized by irregular and steep bathymetry, whereas the region near Fram Strait is broader and deeper, allowing Atlantic waters to recirculate into the Greenland Sea and around the Nordic Seas (Fig. 12). Here, a clear pathway extends across the section, representing the recirculation of waters into the Greenland Sea with mean velocities below $6\,\mathrm{cm\,s^{-1}}$, following the branches of Atlantic water (Fig. 12b,c). Numerical simulations have shown that the waters that manage to cross the ridge are then transformed via cooling and freshening (Ypma et al., 2020). The study of Ypma et al. (2020) also show significant exchange across the Knipovitch Ridge at the surface due to the instability of the frontal current, while the crossings of Argo floats at mid-depth may be influenced by other mechanisms.

https://doi.org/10.5194/egusphere-2026-7272
Preprint. Discussion started: 25 November 2026
© Author(s) 2026. CC BY 4.0 License.

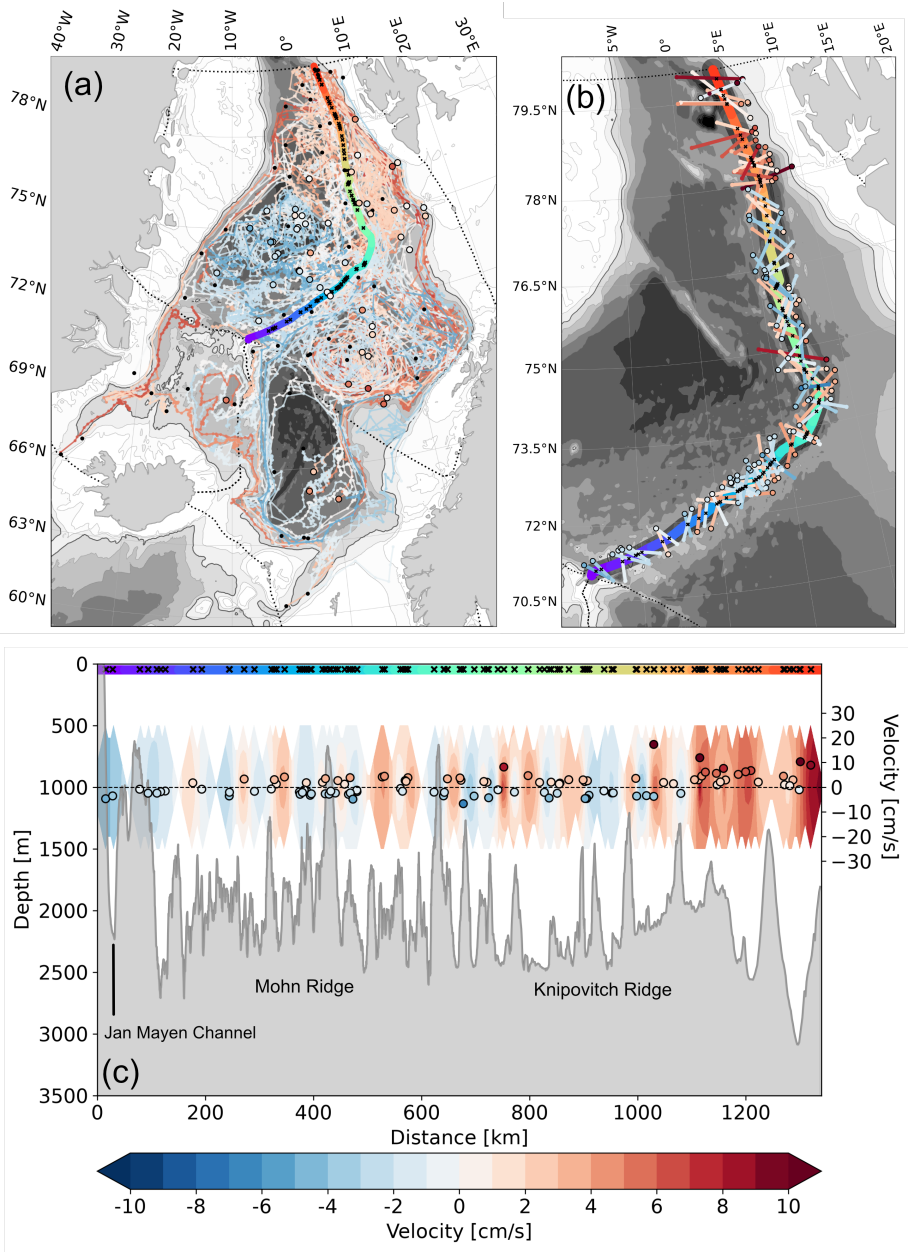

Figure 12. Same as Figure 9 but for the section from Jan Mayen towards Fram Strait. The blue trajectories in (a) and (b) as well as the colours in (c) indicate floats crossing from the Greenland Sea into the Lofoten Basin, and vice versa for the red trajectories. The isobaths in (a) and (b) are the same as for Figure 2.

https://doi.org/10.5194/egusphere-2026-7272
Preprint. Discussion started: 25 November 2026
© Author(s) 2026. CC BY 4.0 License.

5 Seasonal variability

Having identified the mean mid-depth circulation of the Nordic Seas, we next examine its seasonal variability. Seasonal changes in atmospheric forcing can influence the circulation below the surface through wind stress and the associated wind-stress curl. In the Nordic Seas, wind-stress curl exhibits a pronounced seasonal cycle, with stronger cyclonic forcing in winter and weak or near-zero forcing in summer; the seasonal momentum forcing is largest over the Greenland Sea and smallest over the Norwegian Basin (Jónsson, 1991; Voet et al., 2010). Seasonal variations in wind stress and wind-stress curl can therefore modulate the cyclonic Nordic Seas circulation and its exchanges across the Greenland-Scotland Ridge through topographic adjustment and boundary-current dynamics (Bringedal et al., 2018). The North Atlantic Oscillation (NAO) further modulates the regional wind field and wind-stress curl, with positive NAO conditions generally associated with stronger winter winds and changes in the wind-driven circulation (Kolstad, 2008; Serra et al., 2010). Consistent with this forcing, a depressed sea surface height (SSH) anomaly over the central Norwegian Sea is associated with an intensified Norwegian Sea Gyre, whereas an elevated SSH anomaly is associated with a weaker gyre; the gyre is therefore expected to strengthen during winter and positive NAO phases (Hátún et al., 2021). Observational studies have likewise reported enhanced near-surface velocities during winter (Jakobsen et al., 2003), increased winter transport across the Greenland continental slope (Woodgate et al., 1999), and pronounced seasonal variability in the NwAFC along the Mohn Ridge at depths near $1000\,\mathrm{m}$ (Bosse and Fer, 2019).

Our mean seasonal circulation fields show that the largest absolute winter–summer differences in speed occur along the EGC, where winter velocities (November–April) can be more than $3\,\mathrm{cm\,s^{-1}}$ higher than in summer (May–October, Fig. 13c). Throughout the western basins, the wind-stress curl is intensified during winter, while the eastern basins experience comparatively weak local seasonal curl differences (Fig. 13f). Despite this weak local curl contrast, an increase in winter velocities is also observed around the Norwegian Basin, associated with the Norwegian Sea Gyre circulation. This indicates that the seasonal intensification of the gyre is not controlled solely by the local winter–summer difference in wind-stress curl. Consistent with this, Voet et al. (2010) found the smallest local seasonal wind-stress forcing over the Norwegian Basin, yet could explain much of its mid-depth seasonal variability with wind forcing and bottom friction. The wintertime strengthening may therefore reflect basin-scale wind forcing, adjustment through topographic circulation, or a lagged dynamical response, rather than a local instantaneous relationship between wind-stress curl and mid-depth velocity.

Seasonal estimates from Argo trajectories are, however, sensitive to the spatial and temporal distribution of floats. Sampling is particularly limited along boundary currents and during parts of the winter season (e.g., Fig. 3). We therefore use the GLORYS12 reanalysis as a complementary gridded estimate of the seasonal circulation (a detailed comparison is given in Appendix C). The main spatial pattern of the Argo-derived seasonal variability is reproduced by GLORYS12 at approximately $1000\,\mathrm{m}$ depth (Fig. C2). In particular, the reanalysis shows wintertime intensification of similar magnitude along the EGC and other fast-flowing pathways, while the central basin interiors show weak seasonal signals in both datasets (Fig. C2). Although GLORYS12 generally underestimates the Argo-derived mean velocities in parts of the Norwegian and Lofoten basins

https://doi.org/10.5194/egusphere-2026-7272
Preprint. Discussion started: 25 November 2026
© Author(s) 2026. CC BY 4.0 License.

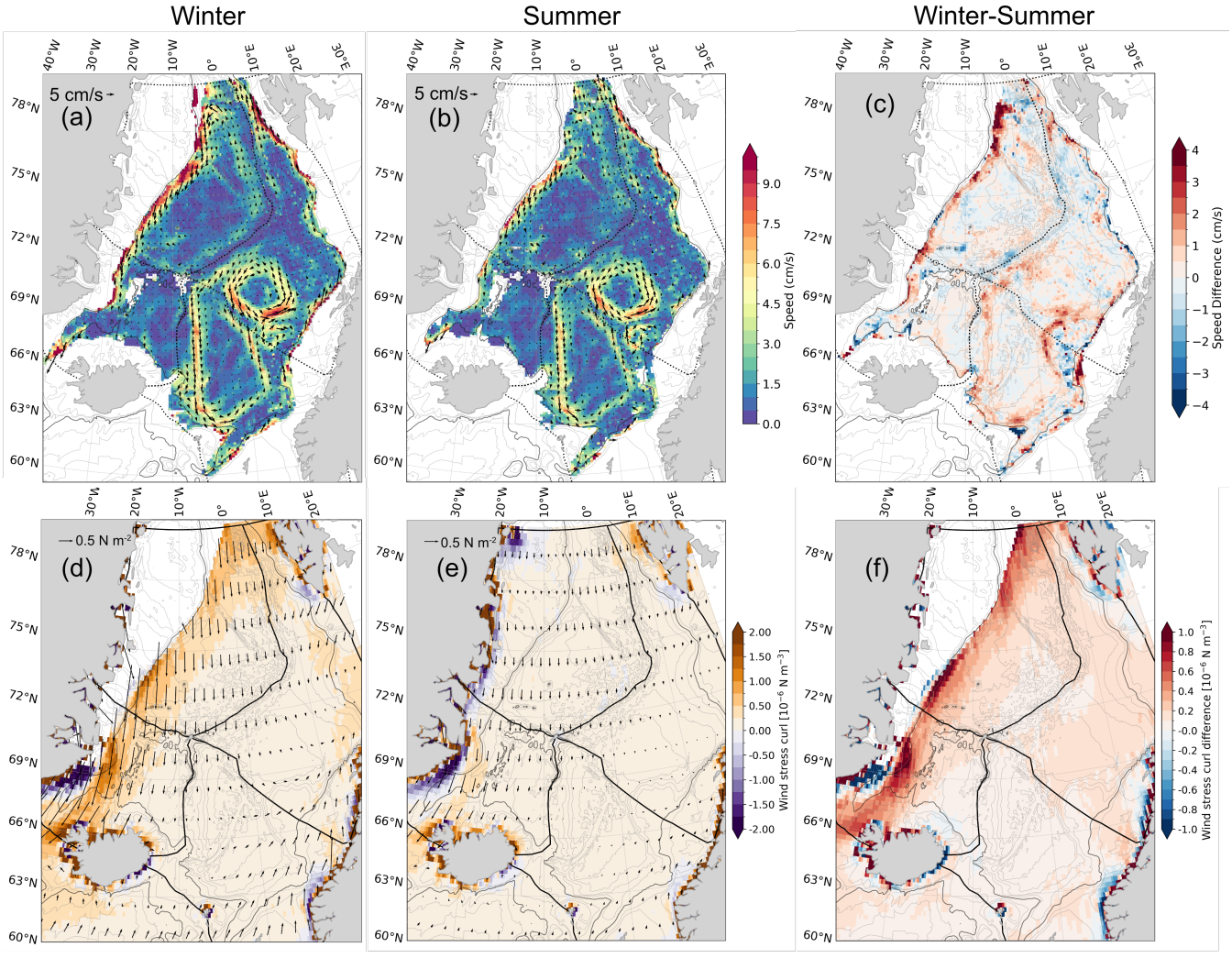

Figure 13. The left (a,d), middle (b,e), and right panels (c,f) show winter circulation (November–April), summer circulation (May–October), and their difference (winter minus summer), respectively. The top row shows the Argo-derived fields and the bottom row shows the corresponding wind stress fields from ERA5. Wind-stress curl is shown as shading in the ERA5 panels, with wind-stress vectors overlaid. The isobaths in all panels are the same as for Figure 2.

(Fig. C1b), the agreement in the location and magnitude of the seasonal signal suggests that the wintertime strengthening is not an artefact of uneven Argo sampling.

https://doi.org/10.5194/egusphere-2026-7272
Preprint. Discussion started: 25 November 2026
© Author(s) 2026. CC BY 4.0 License.

6 Discussion

The Argo trajectories reveal that the mid-depth circulation of the Nordic Seas is strongly shaped by bathymetry. Rather than forming direct pathways between basin interiors and the overflow regions, the circulation is organised into cyclonic basin-scale gyres, with boundary currents providing the principal routes for exchanges between the basins, as summarized in Figure 14. This large-scale pattern is consistent with previous float-based descriptions of the mid-depth Nordic Seas circulation, particularly Voet et al. (2010) who found weak interior flow, stronger flow along basin rims, and limited direct movement of floats between basins. The longer and spatially more extensive Argo record used here extends this picture by providing a broader view of the boundary-current system and interbasin pathways, while also allowing seasonal differences in the mean velocities to be examined.

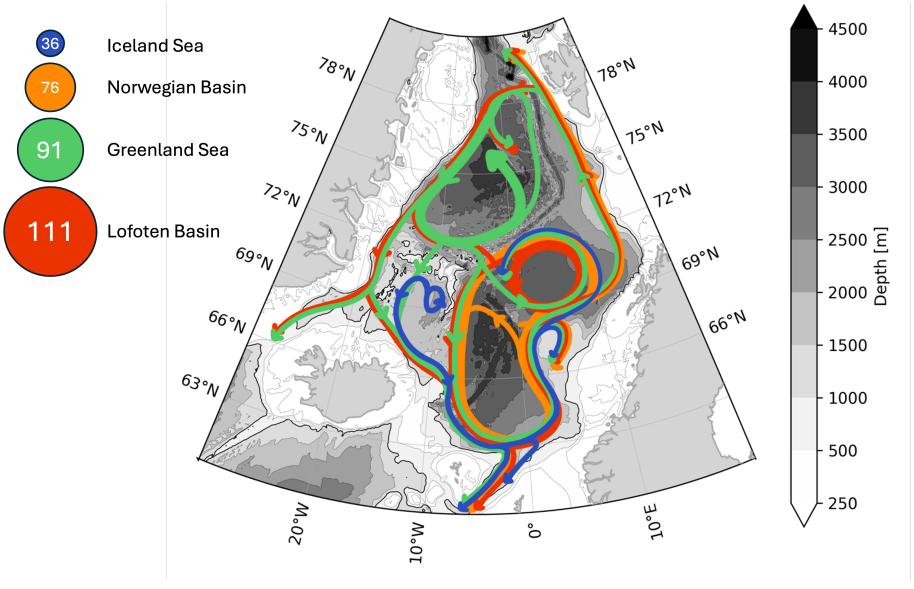

Figure 14. Schematic of the mean mid-depth (1000 m) circulation and interbasin exchange of the Nordic Seas from Argo floats, colour-coded by basin of origin with number of starting floats given in the legend circle size. The line thickness is approximately scaled by the number of floats in each pathway. The isobaths are the same as for Figure 2.

The close association between the circulation and the bathymetry is consistent with the topographic steering expected for a weakly stratified, largely barotropic flow. In particular, Nøst and Isachsen (2003) showed that, at long timescales, bottom currents in the Nordic Seas and Arctic Ocean tend to align with f/H contours, and that a simple diagnostic framework can reproduce major features of the large-scale circulation. The trajectories here further show that interbasin exchange occurs predominantly along boundary currents, whereas direct pathways across the basin interiors are weaker and more sporadic. This emphasizes the role of topographically guided flow in connecting the Nordic Seas basins at mid-depth. Because the floats sample advective pathways at their parking depth, however, they do not resolve all processes contributing to exchange. For example,

https://doi.org/10.5194/egusphere-2026-7272
Preprint. Discussion started: 25 November 2026
© Author(s) 2026. CC BY 4.0 License.

baroclinic eddy fluxes, small-scale mixing and flow through narrow topographic gaps may be underestimated or missed entirely. Spall (2010) highlights the importance of non-local topographic influences, baroclinic instability, and mesoscale eddies for Nordic Seas circulation and water-mass transformation, providing physical context for processes that may not be resolved by the Argo trajectories.

Although the floats drift below the sill depths of the Greenland–Scotland Ridge and therefore do not sample the overflows directly, their pathways help constrain the upstream circulation supplying the overflow regions. Toward the Faroe Bank Channel, the fate of the flow depends strongly on the isobath followed upstream of the channel (Fig. 8). Trajectories following isobaths shallower than approximately $1500\,\mathrm{m}$ tend to be directed toward the channel, whereas trajectories on deeper isobaths tend to recirculate within the Norwegian Basin. A small number of floats overshoot the channel before being redirected southward along the Norwegian slope. Although the sample size is too small to quantify the relative importance of these pathways, this behaviour is consistent with the overflow overshoot and recirculation described by Chafik et al. (2020). Toward Denmark Strait, the sampling is sparser, but no float deployed in the central Iceland Sea reached the strait. Instead, the floats approaching Denmark Strait mainly originated in the Greenland Sea and followed the EGC, with an additional contribution along the northern Icelandic slope consistent with the pathway of the NIJ (Fig. 4). These results suggest that upstream overflow pathways are strongly constrained by topography and by the structure of the boundary-current system, with the Argo floats drifting too deep to adequately capture the full upstream circulation of the overflows.

The seasonal analysis adds a complementary perspective to this mean circulation, with faster circulation in winter compared to summer (Fig.13). Seasonal changes in wind stress and wind-stress curl can modulate the topographically constrained circulation, particularly through basin-scale vorticity forcing and its adjustment through bottom friction and topographic steering. Voet et al. (2010) found that the seasonal variability of the Greenland and Norwegian Basin mid-depth flow can be adequately represented by a barotropic vorticity equation with wind forcing and bottom friction, whereas less of the variance is explained by wind in the Lofoten Basin and over the Iceland Plateau. This framework helps interpret the Norwegian Basin result: although the local winter–summer difference in wind-stress curl is small, the gyre may still intensify in winter because the relevant forcing is not solely the local curl. Basin-integrated wind forcing, topographic adjustment, and lagged dynamical responses can all contribute to a strengthening of the cyclonic rim circulation.

Several limitations arise from the nature of the Argo dataset. Float sampling is spatially and temporally uneven because deployments are concentrated in the deep basin interiors and often occur during summer research cruises. As a result, boundary currents are more sparsely sampled than the basin interiors. Long-term averaging also smooths transient or migrating features. For example, the anticyclonic Lofoten Vortex migrates within the Lofoten Basin rather than remaining stationary (Raj et al., 2015), and is therefore not resolved as a coherent feature in the long-term mean circulation presented here (Fig. 4), although it is present in the GLORYS12 reanalysis (Fig. C1).

https://doi.org/10.5194/egusphere-2026-7272
Preprint. Discussion started: 25 November 2026
© Author(s) 2026. CC BY 4.0 License.

Additional uncertainty arises from the way Argo velocities are estimated. As Argo floats are not continuously tracked while drifting at depth, subsurface velocities must be inferred from the linear displacement between successive surfacing locations. This can underestimate the true drift speed, especially in regions with curved pathways, eddies or complex bathymetry. The estimates also neglect the time spent profiling and at the surface, as well as the vertical shear experienced during ascent and descent. The vertical shear is particularly strong in the Lofoten Basin, with the northward flowing NwAFC and southward flowing deep current along the Mohn Ridge (Fig. 4). Previous studies have estimated uncertainties associated with these effects at approximately $0.25\,\mathrm{cm\,s^{-1}}$ 0.25 to $0.53\,\mathrm{cm\,s^{-1}}$ for displacement-based Argo velocity estimates (Lebedev et al., 2007; Ollitrault and Rannou, 2013; Almeida et al., 2025).

Surface positioning errors provide an additional source of uncertainty, particularly for older floats using less accurate positioning systems (Wong et al., 2025). Comparisons between Argo and acoustically tracked RAFOS floats have not revealed a systematic bias between the two systems (Machín et al., 2006; de Jong et al., 2018), supporting the robustness of the large-scale circulation patterns inferred here. The mean distance travelled by a float over ten days is approximately $40\,\mathrm{km}$, whereas positioning uncertainty is generally of the order of a few hundred metres at most for modern floats, although it may be larger for older positioning systems (Wong et al., 2025). Positioning errors are therefore unlikely to dominate the velocity estimates. Uncertainties associated with profiling, surface drift, vertical shear, and temporal averaging remain more relevant, especially in regions of complex bathymetry or strong mesoscale variability.

Despite these limitations, the Argo record provides the most spatially extensive observational Lagrangian view currently available of the mid-depth Nordic Seas circulation. The results highlight the importance of topographically guided boundary currents for interbasin exchange and for the upstream pathways feeding the overflow regions. Future observational efforts should therefore more directly target the shallower boundary currents, the overflow approaches, and narrow topographic passages. Such observations would complement the Argo-based mid-depth circulation presented here and help close the connection between basin-scale exchange within the Nordic Seas and the dense overflows across the Greenland–Scotland Ridge.

7 Conclusion

This study used 25 years of Argo float trajectories to characterise the mid-depth circulation and interbasin exchange of the Nordic Seas at approximately $1000\,\mathrm{m}$. The results show that the circulation is organised as a connected system of cyclonic basin gyres, boundary currents, and topographically guided pathways. The strongest mean velocities occur along the boundary currents and regions of steep bathymetry, whereas the basin interiors are characterised by weaker mean flow. Some floats are diverted from the steeper boundary regions toward the interior in regions prone to instabilities.

https://doi.org/10.5194/egusphere-2026-7272
Preprint. Discussion started: 25 November 2026
© Author(s) 2026. CC BY 4.0 License.

Interbasin exchange is dominated by the boundary-current system. Direct exchange between the eastern and western basin interiors is limited by the cyclonic gyres, shallow ridges, and hydrographic fronts. Zonal connections are most evident through the recirculation near Fram Strait and between the southern Iceland Sea and the Norwegian Basin. Meridional exchange is mainly associated with the boundary currents The boundary-current system is strongest during winter, when velocities increase by up to $5\,\mathrm{cm\,s^{-1}}$ relative to summer. This seasonal intensification is broadly consistent with stronger winter wind forcing and wind-stress curl, although the response is not controlled solely by the local forcing.

The Argo trajectories identify several possible upstream pathways toward the Greenland–Scotland Ridge, but they do not directly resolve overflow transport due to the shallow sill depths. Flow toward Denmark Strait is mainly associated with the EGC, while pathways toward the Faroe Bank Channel include flow originating in the Iceland Sea, as well as flow that has diverted from the EGC and is steered through the Norwegian Basin toward the Norwegian slope. The floats therefore provide stronger constraints on the upstream mid-depth circulation than on the overflow branches themselves. The observed trajectories indicate that a substantial fraction of the mid-depth flow recirculates within the Nordic Seas, while only a subset follows pathways that approach the Greenland–Scotland Ridge.

The results should be interpreted in light of uneven sampling, velocity uncertainty, and the limited representation of narrow boundary currents, topographic passages, and overflow approaches. The exchange inferred here therefore describes the resolved advective connectivity at the Argo parking depth and does not include all eddy fluxes, small- scale mixing or unresolved flow through narrow gaps. Nevertheless, the Argo record provides a spatially extensive observational view of the mid-depth circulation and demonstrates that connectivity in the Nordic Seas is governed by the interaction between basin-scale recirculation, boundary currents, and topography, rather than by a single continuous pathway from the basin interiors to the overflows.

Data availability. These data were collected and made freely available by the International Argo Program and the national programs that contribute to it (http://www.argo.ucsd.edu, https://ocean-ops.org). The Argo Program is part of the Global Ocean Observing System. Argo (2026). The GLORYS12 reanalysis data used in this study is available at https://doi.org/10.48670/moi-00021. The ERA5 data used in this study are available from the Copernicus Climate Change Service (2023): ERA5 monthly averaged data on single levels from 1940 to present. Copernicus Climate Change Service (C3S) Climate Data Store (CDS). DOI: 10.24381/cds.f17050d7 (Accessed on 10-09-2026).

https://doi.org/10.5194/egusphere-2026-7272
Preprint. Discussion started: 25 November 2026
© Author(s) 2026. CC BY 4.0 License.

Appendix A: Argo float age distribution

Based on all available Argo floats in the Nordic Seas, including those that are still active and those that are inactive, the mean float lifetime in the Nordic Seas is approximately 3.5 years. However, individual floats can remain operational for almost 8 years. (Fig. A1). In the first 6 months since deployment, almost all of the Argo floats remain within their original basin. Some floats start to leave their deployment basin in relatively equal amounts between the Greenland Sea, Norwegian Basin, and Lofoten Sea within the first year. By six years of age, all floats have left their deployment basin or they are no longer active.

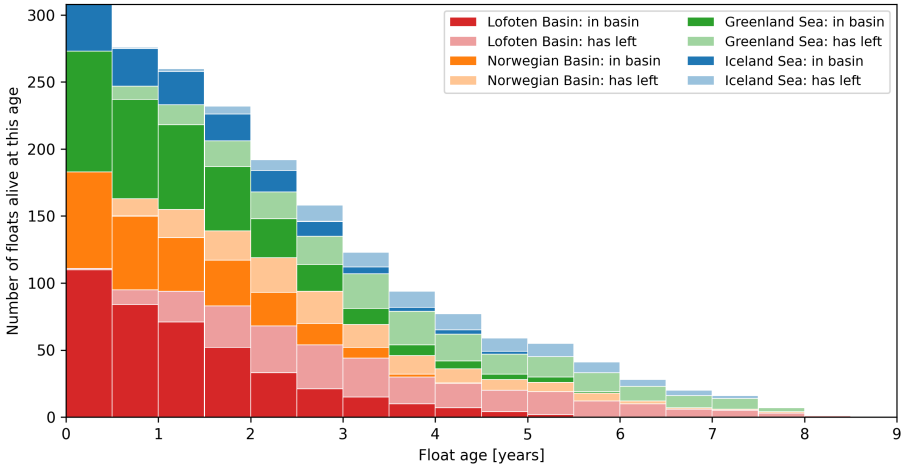

Figure A1. Distribution of floats by age since deployment, coloured by starting basin. The distribution shows the number of floats still active at a certain age and whether they are within their deployment basin (solid colour) or have left (lighter colour).

Appendix B: Mid-depth hydrographic properties

To provide hydrographic context for the mid-depth circulation presented in this study, temperature and salinity Argo profiles between $990\,\mathrm{m}$ and $1010\,\mathrm{m}$ are averaged and gridded anisotropically onto the same grid as the mean velocity field (Section 2). At mid-depth ($1000\,\mathrm{m}$) the hydrographic properties are relatively homogeneous across much of the Nordic Seas (Fig. B1). The main exception is the central Lofoten Basin which contains relatively warm and saline Atlantic waters. Elsewhere, mid-depth waters are generally cold, with temperatures below $0°\mathrm{C}$. Following Rudels et al. (2005), the boundary between Intermediate Water and Deep Water is defined by a potential density anomaly referred to $500\,\mathrm{m}$ depth of $30.444\,\mathrm{kg\,m^{-3}}$ (Fig. B1c). Most of the mid-depth waters sampled here therefore belong to the Intermediate Water class that can more readily supply the overflow waters, whereas denser Deep Waters are more confined to the deeper parts of the basins and certain regions along the eastern boundary.

https://doi.org/10.5194/egusphere-2026-7272
Preprint. Discussion started: 25 November 2026
© Author(s) 2026. CC BY 4.0 License.

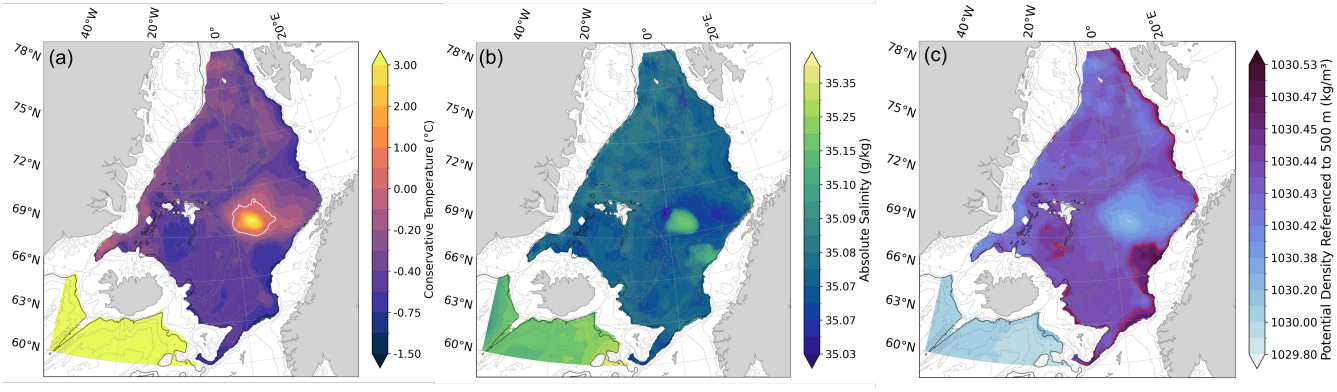

Figure B1. 1000 m gridded Argo profile data of (a) Conservative Temperature with 0°C isotherm contoured in white, (b) Absolute Salinity, (c) potential density anomaly referenced to 500 m depth with the 30.444 kg m^{-3} contoured in red separating the Intermediate Water (lighter than this threshold) from the Deep Water (Rudels et al., 2005).

Appendix C: GLORYS12 reanalysis mean circulation and seasonality

To provide an independent, gridded estimate of the mean and seasonal mid-depth circulation, we compare Argo-derived velocities with the GLORYS12 reanalysis. GLORYS12 assimilates along-track altimetry, satellite sea-surface temperatures, sea-ice concentration, and in situ temperature and salinity profiles, including Argo profiles, but does not assimilate the subsurface velocities derived from Argo float displacements (Lellouche et al., 2021; Wong et al., 2025). The comparison therefore evaluates whether the reanalysis reproduces the circulation inferred independently from the Argo trajectories. GLORYS12 represents the hydrography of the Nordic Seas reasonably well compared with historical observations (Huang et al., 2023; Chafik et al., 2023; Mayer et al., 2023; Årthun et al., 2025).

The surface velocities from GLORYS12 (Fig. C1a) show circulation patterns consistent with observations in the Nordic Seas (Poulain et al., 1996; Jakobsen et al., 2003), with strong boundary currents reaching up to 30 cm s^{-1} and relatively weak interior flow. We also compare the 500 m GLORYS12 mean velocity field (not shown) with the surface and mid-depth (1000 m) circulation over the same period. Consistent with the largely barotropic nature of the flow, the 500 m circulation follows similar pathways to the mid-depth circulation, except from the branch flowing northwards along the Mohn Ridge, which resembles the surface circulation (Fig. C1a). However, GLORYS12 slightly underestimates the Argo-derived mid-depth mean velocities, especially in the Norwegian and Lofoten gyres, although the EGC is relatively well-represented with velocities exceeding 10 cm s^{-1} (Fig. C1b). The Argo-derived mean velocities show coherent meridional flow along the Mohn and Knipovitch ridges that is absent in the GLORYS12 fields. Within the Lofoten Basin, the Lofoten Vortex is more clearly defined in GLORYS12, whereas the deep cyclonic gyre is more prominent in the Argo observations.

https://doi.org/10.5194/egusphere-2026-7272
Preprint. Discussion started: 25 November 2026
© Author(s) 2026. CC BY 4.0 License.

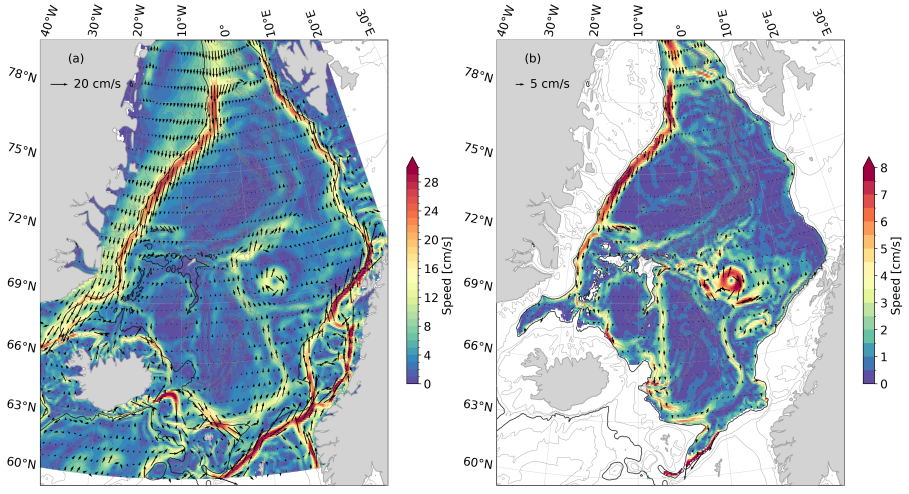

Figure C1. Mean (a) surface and (b) mid-depth (1000 m) circulation from GLORYS12 (2001 to 2026).

At 1000 m, the GLORYS12 fields reproduce the main locations of wintertime intensification and simulate seasonal differences of a similar order of magnitude to the Argo velocities (Figs. C2 and 13). The agreement is clearest along the EGC and other fast-flowing pathways, including some pathways within the interior basins, whereas the central parts of the deep basins show weak seasonal signals in both datasets. The GLORYS12 winter-summer velocity difference reaches up to approximately $4\,\mathrm{cm\,s^{-1}}$ along these fast-flowing pathways, which is similar to the corresponding Argo-derived difference. Thus, despite its weaker mean velocities, GLORYS12 captures the main spatial structure of the seasonal variability of the Nordic Seas.

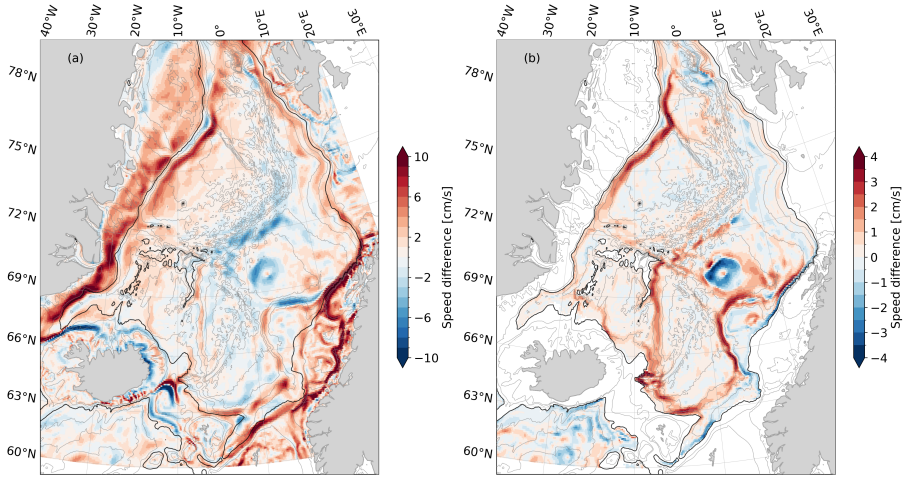

Figure C2. Winter minus summer mean velocities for (a) surface and (b) 1000 m circulation from GLORYS12 reanalysis from January 2001 to May 2026.

https://doi.org/10.5194/egusphere-2026-7272
Preprint. Discussion started: 25 November 2026
© Author(s) 2026. CC BY 4.0 License.

Author contributions. Conceptualization: E. Giorgi, K, Våge, S. Semper. Formal analysis: E.G. Funding acquisition: K.V. Methodology: E.G. Project administration: K.V. Supervision: K.V, S.S, I.F. Visualization: E.G. Writing - original draft: E.G. Writing - review and editing: E.G., K.V., S.S., I.F, A-M.S., A.B.

Competing interests. At least one of the (co-)authors is a member of the editorial board of Ocean Science.

Acknowledgements. This project received funding from the European Union under the ERC Grant Agreement 101088452 (ROVER; K.V., S.S., A.B., and A.-M.S.).

https://doi.org/10.5194/egusphere-2026-7272
Preprint. Discussion started: 25 November 2026
© Author(s) 2026. CC BY 4.0 License.

References

Almeida, L., Lique, C., Kolodziejczyk, N., and Desbruyères, D.: Drivers of Water Mass Volume Changes in the Nordic Seas (2005–2020), Journal of Geophysical Research: Oceans, 130, e2024JC022 209, https://doi.org/10.1029/2024JC022209, 2025.

Amante, C. and Eakins, B.: ETOPO1 1 Arc-Minute Global Relief Model., https://doi.org/10.7289/V5C8276M, 2009.

Argo: Argo float data and metadata from Global Data Assembly Centre (Argo GDAC), https://doi.org/10.17882/42182, 2026.

Bosse, A. and Fer, I.: Mean Structure and Seasonality of the Norwegian Atlantic Front Current Along the Mohn Ridge From Repeated Glider Transects, Geophysical Research Letters, 46, 13 170–13 179, https://doi.org/10.1029/2019GL084723, _eprint: https://agupubs.onlinelibrary.wiley.com/doi/pdf/10.1029/2019GL084723, 2019.

Bosse, A., Fer, I., Søiland, H., and Rossby, T.: Atlantic Water Transformation Along Its Poleward Pathway Across the Nordic Seas, Journal of Geophysical Research: Oceans, 123, 6428–6448, https://doi.org/10.1029/2018JC014147, 2018.

Bourke, R. H., Paquette, R. G., and Blythe, R. F.: The Jan Mayen Current of the Greenland Sea, Journal of Geophysical Research: Oceans, 97, 7241–7250, https://doi.org/10.1029/92JC00150, 1992.

Brakstad, A., Gebbie, G., Våge, K., Jeansson, E., and Ólafsdóttir, S. R.: Formation and pathways of dense water in the Nordic Seas based on a regional inversion, Progress in Oceanography, 212, 102 981, https://doi.org/10.1016/j.pocean.2023.102981, 2023.

Bringedal, C., Eldevik, T., Skagseth, , Spall, M. A., and Østerhus, S.: Structure and Forcing of Observed Exchanges across the Greenland–Scotland Ridge, Journal of Climate, 31, 9881–9901, https://doi.org/10.1175/JCLI-D-17-0889.1, 2018.

Casanova-Masjoan, M., Pérez-Hernández, M. D., Pickart, R. S., Valdimarsson, H., Ólafsdóttir, S. R., Macrander, A., Grisolía-Santos, D., Torres, D. J., Jónsson, S., Våge, K., Lin, P., and Hernández-Guerra, A.: Along-Stream, Seasonal, and Interannual Variability of the North Icelandic Irminger Current and East Icelandic Current Around Iceland, Journal of Geophysical Research: Oceans, 125, e2020JC016 283, https://doi.org/10.1029/2020JC016283, 2020.

Chafik, L., Nilsen, J. E. , Dangendorf, S., Reverdin, G., and Frederikse, T.: North Atlantic Ocean Circulation and Decadal Sea Level Change During the Altimetry Era, Scientific Reports, 9, 1041, https://doi.org/10.1038/s41598-018-37603-6, 2019.

Chafik, L., Hátún, H., Kjellsson, J., Larsen, K. M. H., Rossby, T., and Berx, B.: Discovery of an unrecognized pathway carrying overflow waters toward the Faroe Bank Channel, Nature Communications, 11, 3721, https://doi.org/10.1038/s41467-020-17426-8, 2020.

Chafik, L., Nilsson, J., Rossby, T., and Kondetharayil Soman, A.: The Faroe-Shetland Channel Jet: Structure, Variability, and Driving Mechanisms, Journal of Geophysical Research: Oceans, 128, e2022JC019 083, https://doi.org/10.1029/2022JC019083, 2023.

de Jong, M. F., Søiland, H., Bower, A. S., and Furey, H. H.: The subsurface circulation of the Iceland Sea observed with RAFOS floats, Deep Sea Research Part I: Oceanographic Research Papers, 141, 1–10, https://doi.org/10.1016/j.dsr.2018.07.008, 2018.

Dundas, V. and Fer, I.: Atlantic Water flow through Fram Strait to the Arctic Ocean measured by repeated glider transects, Ocean Science, 22, 1003–1021, https://doi.org/10.5194/os-22-1003-2026, 2026.

Evans, D. G., Holliday, N. P., Bacon, S., and Le Bras, I.: Mixing and air–sea buoyancy fluxes set the time-mean overturning circulation in the subpolar North Atlantic and Nordic Seas, Ocean Science, 19, 745–768, https://doi.org/10.5194/os-19-745-2023, 2023.

Hansen, B. and Østerhus, S.: North Atlantic–Nordic Seas exchanges, Progress in Oceanography, 45, 109–208, https://doi.org/10.1016/S0079-6611(99)00052-X, 2000.

Hersbach, H., Bell, B., Berrisford, P., Hirahara, S., Horányi, A., Muñoz-Sabater, J., Nicolas, J., Peubey, C., Radu, R., Schepers, D., Simmons, A., Soci, C., Abdalla, S., Abellan, X., Balsamo, G., Bechtold, P., Biavati, G., Bidlot, J., Bonavita, M., De Chiara, G., Dahlgren, P., Dee, D., Diamantakis, M., Dragani, R., Flemming, J., Forbes, R., Fuentes, M., Geer, A., Haimberger, L., Healy, S., Hogan, R. J.,

https://doi.org/10.5194/egusphere-2026-7272
Preprint. Discussion started: 25 November 2026
© Author(s) 2026. CC BY 4.0 License.

Hólm, E., Janisková, M., Keeley, S., Laloyaux, P., Lopez, P., Lupu, C., Radnoti, G., de Rosnay, P., Rozum, I., Vamborg, F., Villaume, S., and Thépaut, J.-N.: The ERA5 global reanalysis, Quarterly Journal of the Royal Meteorological Society, 146, 1999–2049, https://doi.org/10.1002/qj.3803, 2020.

Holloway, G., Dupont, F., Golubeva, E., Häkkinen, S., Hunke, E., Jin, M., Karcher, M., Kauker, F., Maltrud, M., Morales Maqueda, M. A., Maslowski, W., Platov, G., Stark, D., Steele, M., Suzuki, T., Wang, J., and Zhang, J.: Water properties and circulation in Arctic Ocean models, Journal of Geophysical Research: Oceans, 112, https://doi.org/10.1029/2006JC003642, 2007.

Huang, J., Pickart, R. S., Huang, R. X., Lin, P., Brakstad, A., and Xu, F.: Sources and upstream pathways of the densest overflow water in the Nordic Seas, Nature Communications, 11, 5389, https://doi.org/10.1038/s41467-020-19050-y, 2020.

Huang, J., Pickart, R. S., Chen, Z., and Huang, R. X.: Role of air-sea heat flux on the transformation of Atlantic Water encircling the Nordic Seas, Nature Communications, 14, 141, https://doi.org/10.1038/s41467-023-35889-3, 2023.

Hátún, H., Chafik, L., and Larsen, K. M. H.: The Norwegian Sea Gyre – A Regulator of Iceland-Scotland Ridge Exchanges, Frontiers in Marine Science, 8, 694 614, https://doi.org/10.3389/fmars.2021.694614, 2021.

Håvik, L., Pickart, R. S., Våge, K., Torres, D., Thurnherr, A. M., Beszczynska-Möller, A., Walczowski, W., and Von Appen, W.: Evolution of the East Greenland Current from Fram Strait to Denmark Strait: Synoptic measurements from summer 2012, Journal of Geophysical Research: Oceans, 122, 1974–1994, https://doi.org/10.1002/2016JC012228, 2017.

Håvik, L., Almansi, M., Våge, K., and Haine, T. W. N.: Atlantic-Origin Overflow Water in the East Greenland Current, Journal of Physical Oceanography, 49, 2255–2269, https://doi.org/10.1175/JPO-D-18-0216.1, 2019.

Isachsen, P. E., Mauritzen, C., and Svendsen, H.: Dense water formation in the Nordic Seas diagnosed from sea surface buoyancy fluxes, Deep Sea Research Part I: Oceanographic Research Papers, 54, 22–41, https://doi.org/10.1016/j.dsr.2006.09.008, 2007.

Jakobsen, P. K., Ribergaard, M. H., Quadfasel, D., Schmith, T., and Hughes, C. W.: Near-surface circulation in the northern North Atlantic as inferred from Lagrangian drifters: Variability from the mesoscale to interannual, Journal of Geophysical Research: Oceans, 108, 2002JC001 554, https://doi.org/10.1029/2002JC001554, 2003.

Jeansson, E., Jutterström, S., Rudels, B., Anderson, L. G., Anders Olsson, K., Jones, E. P., Smethie, W. M., and Swift, J. H.: Sources to the East Greenland Current and its contribution to the Denmark Strait Overflow, Progress in Oceanography, 78, 12–28, https://doi.org/10.1016/j.pocean.2007.08.031, 2008.

Johnston, T. M. S., Sjur, A. L. P., Isachsen, P. E., and LaCasce, J. H.: Eddy- and Wind-Driven Circulation in the Enclosed Basins of the Norwegian Sea Evaluated Using a Model and Absolute Geostrophic Flow From Argo, Journal of Geophysical Research: Oceans, 130, e2024JC021 990, https://doi.org/10.1029/2024JC021990, 2025.

Jónsson, S.: Seasonal and interannual variability of wind stress curl over the Nordic Seas, Journal of Geophysical Research: Oceans, 96, 2649–2659, https://doi.org/10.1029/90JC02230, 1991.

Killworth, P. D.: Deep convection in the World Ocean, Reviews of Geophysics, 21, 1–26, https://doi.org/10.1029/RG021i001p00001, 1983.

Killworth, P. D.: An Equivalent-Barotropic Mode in the Fine Resolution Antarctic Model, https://journals.ametsoc.org/view/journals/phoc/22/11/1520-0485_1992_022_1379_aebmit_2_0_co_2.xml, 1992.

Kolstad, E. W.: A QuikSCAT climatology of ocean surface winds in the Nordic seas: Identification of features and comparison with the NCEP/NCAR reanalysis, Journal of Geophysical Research: Atmospheres, 113, 2007JD008 918, https://doi.org/10.1029/2007JD008918, 2008.

Kuhlbrodt, T., Griesel, A., Montoya, M., Levermann, A., Hofmann, M., and Rahmstorf, S.: On the driving processes of the Atlantic meridional overturning circulation, Reviews of Geophysics, 45, https://doi.org/10.1029/2004RG000166, 2007.

https://doi.org/10.5194/egusphere-2026-7272
Preprint. Discussion started: 25 November 2026
© Author(s) 2026. CC BY 4.0 License.

LaCasce, J. H.: Floats and f/H, Journal of Marine Research, 58, 61–95, https://doi.org/10.1357/002224000321511205, 2000.

Lebedev, K., Yoshinari, H., Maximenko, N., and Hacker, P.: (PDF) YoMaHa'07: Velocity data assessed from trajectories of Argo floats at parking level and at the sea surface, https://doi.org/10.13140/RG.2.2.12820.71041, 2007.

Lellouche, J.-M., Greiner, E., Bourdallé-Badie, R., Garric, G., Melet, A., MaDrévillonrie, M., Bricaud, C., Belbéoch, M., Le Galloudec, O., Regnier, C., Candela, T., Testut, C.-E., Gasparin, F., Ruggiero, G., Benkiran, M., Drillet, Y., and Le Traon, P.-Y.: The Copernicus Global 1/12° Oceanic and Sea Ice GLORYS12 Reanalysis, Frontiers in Earth Science, 9, https://doi.org/10.3389/feart.2021.698876, 2021.

Lozier, M. S.: Overturning in the subpolar North Atlantic: a review, Philosophical Transactions of the Royal Society A: Mathematical, Physical and Engineering Sciences, 381, 20220 191, https://doi.org/10.1098/rsta.2022.0191, 2023.

Machín, F., Send, U., and Zenk, W.: Intercomparing drifts from RAFOS and profiling floats in the deep western boundary current along the Mid-Atlantic Ridge, Scientia Marina, 70, 1–8, https://doi.org/10.3989/scimar.2006.70n11, 2006.

Macrander, A., Valdimarsson, H., and Jónsson, S.: Improved transport estimate of the East Icelandic Current 2002–2012, Journal of Geophysical Research: Oceans, 119, 3407–3424, https://doi.org/10.1002/2013JC009517, 2014.

Marshall, J. and Schott, F.: Open-ocean convection: Observations, theory, and models, Reviews of Geophysics, 37, 1–64, https://doi.org/10.1029/98RG02739, 1999.

Mauritzen, C.: Production of dense overflow waters feeding the North Atlantic across the Greenland-Scotland Ridge. Part 1: Evidence for a revised circulation scheme, Deep Sea Research Part I: Oceanographic Research Papers, 43, 769–806, https://doi.org/10.1016/0967-0637(96)00037-4, 1996.

Mayer, M., Tsubouchi, T., Winkelbauer, S., Larsen, K. M. H., Berx, B., Macrander, A., Iovino, D., Jónsson, S., and Renshaw, R.: Recent variations in oceanic transports across the Greenland–Scotland Ridge, State of the Planet, 1-osr7, 1–13, https://doi.org/10.5194/sp-1-osr7-14-2023, 2023.

Moe, T. , Daae, K., Våge, K., and Semper, S.: An Idealized Model for the Emergence of the North Icelandic Jet, Journal of Geophysical Research: Oceans, 130, e2024JC021 992, https://doi.org/10.1029/2024JC021992, 2025.

Mork, K. A., Drinkwater, K. F., Jónsson, S., Valdimarsson, H., and Ostrowski, M.: Water mass exchanges between the Norwegian and Iceland seas over the Jan Mayen Ridge using in-situ current measurements, Journal of Marine Systems, 139, 227–240, https://doi.org/10.1016/j.jmarsys.2014.06.008, 2014.

Nurser, A. J. G. and Bacon, S.: The Rossby radius in the Arctic Ocean, Ocean Science, 10, 967–975, https://doi.org/10.5194/os-10-967-2014, 2014.

Nøst, O. A. and Isachsen, P. E.: The large-scale time-mean ocean circulation in the Nordic Seas and Arctic Ocean estimated from simplified dynamics, Journal of Marine Research, 61, 175–210, https://doi.org/10.1357/002224003322005069, 2003.

Ollitrault, M. and Rannou, J.-P.: ANDRO: An Argo-Based Deep Displacement Dataset, Journal of Atmospheric and Oceanic Technology, 30, 759–788, https://doi.org/10.1175/JTECH-D-12-00073.1, 2013.

Orvik, K. A. and Niiler, P.: Major pathways of Atlantic water in the northern North Atlantic and Nordic Seas toward Arctic, Geophysical Research Letters, 29, 2–1–2–4, https://doi.org/10.1029/2002GL015002, 2002.

Pellichero, V., Lique, C., Kolodziejczyk, N., and Balem, K.: Structure and Variability of the Jan Mayen Current in the Greenland Sea Gyre From a Yearlong Mooring Array, Journal of Geophysical Research: Oceans, 128, e2022JC019 616, https://doi.org/10.1029/2022JC019616, 2023.

Pickart, R. S. and Smethie, W. M.: Temporal evolution of the deep western boundary current where it enters the sub-tropical domain, Deep Sea Research Part I: Oceanographic Research Papers, 45, 1053–1083, https://doi.org/10.1016/S0967-0637(97)00084-8, 1998.

https://doi.org/10.5194/egusphere-2026-7272
Preprint. Discussion started: 25 November 2026
© Author(s) 2026. CC BY 4.0 License.

Poulain, P.-M., Warn-Varnas, A., and Niiler, P. P.: Near-surface circulation of the Nordic seas as measured by Lagrangian drifters, Journal of Geophysical Research: Oceans, 101, 18 237–18 258, https://doi.org/10.1029/96JC00506, 1996.

Raj, R. P., Chafik, L., Nilsen, J. E. , Eldevik, T., and Halo, I.: The Lofoten Vortex of the Nordic Seas, Deep Sea Research Part I: Oceanographic Research Papers, 96, 1–14, https://doi.org/10.1016/j.dsr.2014.10.011, 2015.

Roemmich, D., Alford, M. H., Claustre, H., Johnson, K., King, B., Moum, J., Oke, P., Owens, W. B., Pouliquen, S., Purkey, S., Scanderbeg, M., Suga, T., Wijffels, S., Zilberman, N., Bakker, D., Baringer, M., Belbeoch, M., Bittig, H. C., Boss, E., Calil, P., Carse, F., Carval, T., Chai, F., Conchubhair, D. , d'Ortenzio, F., Dall'Olmo, G., Desbruyeres, D., Fennel, K., Fer, I., Ferrari, R., Forget, G., Freeland, H., Fujiki, T., Gehlen, M., Greenan, B., Hallberg, R., Hibiya, T., Hosoda, S., Jayne, S., Jochum, M., Johnson, G. C., Kang, K., Kolodziejczyk, N., Körtzinger, A., Traon, P.-Y. L., Lenn, Y.-D., Maze, G., Mork, K. A., Morris, T., Nagai, T., Nash, J., Garabato, A. N., Olsen, A., Pattabhi, R. R., Prakash, S., Riser, S., Schmechtig, C., Schmid, C., Shroyer, E., Sterl, A., Sutton, P., Talley, L., Tanhua, T., Thierry, V., Thomalla, S., Toole, J., Troisi, A., Trull, T. W., Turton, J., Velez-Belchi, P. J., Walczowski, W., Wang, H., Wanninkhof, R., Waterhouse, A. F., Waterman, S., Watson, A., Wilson, C., Wong, A. P. S., Xu, J., and Yasuda, I.: On the Future of Argo: A Global, Full-Depth, Multi-Disciplinary Array, Frontiers in Marine Science, 6, https://doi.org/10.3389/fmars.2019.00439, 2019.

Rossby, T., Ozhigin, V., Ivshin, V., and Bacon, S.: An isopycnal view of the Nordic Seas hydrography with focus on properties of the Lofoten Basin, Deep Sea Research Part I: Oceanographic Research Papers, 56, 1955–1971, https://doi.org/10.1016/j.dsr.2009.07.005, 2009.

Rudels, B., Björk, G., Nilsson, J., Winsor, P., Lake, I., and Nohr, C.: The interaction between waters from the Arctic Ocean and the Nordic Seas north of Fram Strait and along the East Greenland Current: results from the Arctic Ocean-02 Oden expedition, Journal of Marine Systems, 55, 1–30, https://doi.org/10.1016/j.jmarsys.2004.06.008, 2005.

Semper, S., Våge, K., Pickart, R. S., Valdimarsson, H., Torres, D. J., and Jónsson, S.: The Emergence of the North Icelandic Jet and Its Evolution from Northeast Iceland to Denmark Strait, Journal of Physical Oceanography, 49, 2499–2521, https://doi.org/10.1175/JPO-D-19-0088.1, 2019.

Semper, S., Pickart, R. S., Våge, K., Larsen, K. M. H., Hátún, H., and Hansen, B.: The Iceland-Faroe Slope Jet: a conduit for dense water toward the Faroe Bank Channel overflow, Nature Communications, 11, 5390, https://doi.org/10.1038/s41467-020-19049-5, number: 1, 2020.

Semper, S., Våge, K., Pickart, R. S., Jónsson, S., and Valdimarsson, H.: Evolution and Transformation of the North Icelandic Irminger Current Along the North Iceland Shelf, Journal of Geophysical Research: Oceans, 127, e2021JC017 700, https://doi.org/10.1029/2021JC017700, 2022.

Serra, N., Käse, R. H., Kähl, A., Stammer, D., and Quadfasel, D.: On the low-frequency phase relation between the Denmark Strait and the Faroe-Bank Channel overflows, Tellus A: Dynamic Meteorology and Oceanography, 62, 530–550, https://doi.org/10.1111/j.1600-0870.2009.00445.x, 2010.

Spall, M. A.: Boundary Currents and Watermass Transformation in Marginal Seas, https://journals.ametsoc.org/view/journals/phoc/34/5/1520-0485_2004_034_1197_bcawti_2.0.co_2.xml, 2004.

Spall, M. A.: Non-local topographic influences on deep convection: An idealized model for the Nordic Seas, Ocean Modelling, 32, 72–85, https://doi.org/10.1016/j.ocemod.2009.10.009, 2010.

Spall, M. A., Almansi, M., Huang, J., Haine, T. W., and Pickart, R. S.: Lateral redistribution of heat and salt in the Nordic Seas, Progress in Oceanography, 196, 102 609, https://doi.org/10.1016/j.pocean.2021.102609, 2021.

Strass, V. H., Fahrbach, E., Schauer, U., and Sellmann, L.: Formation of Denmark Strait overflow water by mixing in the East Greenland Current, Journal of Geophysical Research: Oceans, 98, 6907–6919, https://doi.org/10.1029/92JC02732, 1993.

https://doi.org/10.5194/egusphere-2026-7272
Preprint. Discussion started: 25 November 2026
© Author(s) 2026. CC BY 4.0 License.

Strehl, A.-M., Våge, K., Smedsrud, L. H., and Barreyre, T.: A 70-year perspective on water-mass transformation in the Greenland Sea: From thermobaric to thermal convection, Progress in Oceanography, 227, 103 304, https://doi.org/10.1016/j.pocean.2024.103304, 2024.

Swift, J. H. and Aagaard, K.: Seasonal transitions and water mass formation in the Iceland and Greenland seas, Deep Sea Research Part A. Oceanographic Research Papers, 28, 1107–1129, https://doi.org/10.1016/0198-0149(81)90050-9, 1981.

Swift, J. H., Aagaard, K., and Malmberg, S.-A.: The contribution of the Denmark strait overflow to the deep North Atlantic, Deep Sea Research Part A. Oceanographic Research Papers, 27, 29–42, https://doi.org/10.1016/0198-0149(80)90070-9, 1980.

Søiland, H., Prater, M. D., and Rossby, T.: Rigid topographic control of currents in the Nordic Seas, Geophysical Research Letters, 35, 2008GL034 846, https://doi.org/10.1029/2008GL034846, 2008.

Tsubouchi, T., Våge, K., Hansen, B., Larsen, K. M. H., Østerhus, S., Johnson, C., Jónsson, S., and Valdimarsson, H.: Increased ocean heat transport into the Nordic Seas and Arctic Ocean over the period 1993–2016, Nature Climate Change, 11, 21–26, https://doi.org/10.1038/s41558-020-00941-3, 2021.

Voet, G., Quadfasel, D., Mork, K. A., and Søiland, H.: The mid-depth circulation of the Nordic Seas derived from profiling float observations, Tellus A, 62, 516–529, https://doi.org/10.1111/j.1600-0870.2010.00444.x, 2010.

Våge, K., Pickart, R. S., Spall, M. A., Valdimarsson, H., Jónsson, S., Torres, D. J., Østerhus, S., and Eldevik, T.: Significant role of the North Icelandic Jet in the formation of Denmark Strait overflow water, Nature Geoscience, 4, 723–727, https://doi.org/10.1038/ngeo1234, number: 10, 2011.

Våge, K., Moore, G. W. K., Jónsson, S., and Valdimarsson, H.: Water mass transformation in the Iceland Sea, Deep Sea Research Part I: Oceanographic Research Papers, 101, 98–109, https://doi.org/10.1016/j.dsr.2015.04.001, 2015.

Wang, X., Zhao, J., Hattermann, T., Lin, L., and Chen, P.: Transports and Accumulations of Greenland Sea Intermediate Waters in the Norwegian Sea, Journal of Geophysical Research: Oceans, 126, e2020JC016 582, https://doi.org/10.1029/2020JC016582, 2021.

Wong, A., Keeley, R., Carval, T., and Team, A. D. M.: Argo Quality Control Manual for CTD and Trajectory Data, Ifremer, https://doi.org/10.13155/33951, version Number: 3.9, 2025.

Wong, A. P. S., Wijffels, S. E., Riser, S. C., Pouliquen, S., Hosoda, S., Roemmich, D., Gilson, J., Johnson, G. C., Martini, K., Murphy, D. J., Scanderbeg, M., Bhaskar, T. V. S. U., Buck, J. J. H., Merceur, F., Carval, T., Maze, G., Cabanes, C., André, X., Poffa, N., Yashayaev, I., Barker, P. M., Guinehut, S., Belbéoch, M., Ignaszewski, M., Baringer, M. O., Schmid, C., Lyman, J. M., McTaggart, K. E., Purkey, S. G., Zilberman, N., Alkire, M. B., Swift, D., Owens, W. B., Jayne, S. R., Hersh, C., Robbins, P., West-Mack, D., Bahr, F., Yoshida, S., Sutton, P. J. H., Cancouët, R., Coatanoan, C., Dobbler, D., Juan, A. G., Gourrion, J., Kolodziejczyk, N., Bernard, V., Bourlès, B., Claustre, H., D'Ortenzio, F., Le Reste, S., Le Traon, P.-Y., Rannou, J.-P., Saout-Grit, C., Speich, S., Thierry, V., Verbrugge, N., Angel-Benavides, I. M., Klein, B., Notarstefano, G., Poulain, P.-M., Vélez-Belchí, P., Suga, T., Ando, K., Iwasaska, N., Kobayashi, T., Masuda, S., Oka, E., Sato, K., Nakamura, T., Sato, K., Takatsuki, Y., Yoshida, T., Cowley, R., Lovell, J. L., Oke, P. R., van Wijk, E. M., Carse, F., Donnelly, M., Gould, W. J., Gowers, K., King, B. A., Loch, S. G., Mowat, M., Turton, J., Rama Rao, E. P., Ravichandran, M., Freeland, H. J., Gaboury, I., Gilbert, D., Greenan, B. J. W., Ouellet, M., Ross, T., Tran, A., Dong, M., Liu, Z., Xu, J., Kang, K., Jo, H., Kim, S.-D., and Park, H.-M.: Argo Data 1999–2019: Two Million Temperature-Salinity Profiles and Subsurface Velocity Observations From a Global Array of Profiling Floats, Frontiers in Marine Science, 7, https://doi.org/10.3389/fmars.2020.00700, 2020.

Woodgate, R. A., Fahrbach, E., and Rohardt, G.: Structure and transports of the East Greenland Current at 75°N from moored current meters, Journal of Geophysical Research: Oceans, 104, 18 059–18 072, https://doi.org/10.1029/1999JC900146, 1999.

Yang, J. and Pratt, L. J.: On the Effective Capacity of the Dense-Water Reservoir for the Nordic Seas Overflow: Some Effects of Topography and Wind Stress, https://doi.org/10.1175/JPO-D-12-087.1, 2013.

https://doi.org/10.5194/egusphere-2026-7272
Preprint. Discussion started: 25 November 2026
© Author(s) 2026. CC BY 4.0 License.



Ypma, S. L., Georgiou, S., Dugstad, J. S., Pietrzak, J. D., and Katsman, C. A.: Pathways and Water Mass Transformation Along and Across the Mohn-Knipovich Ridge in the Nordic Seas, Journal of Geophysical Research: Oceans, 125, https://doi.org/10.1029/2020JC016075, 2020.

Årthun, M., Brakstad, A., Dörr, J., Johnson, H. L., Mans, C., Semper, S., and Våge, K.: Atlantification drives recent strengthening of the Arctic overturning circulation, Science Advances, 11, eadu1794, https://doi.org/10.1126/sciadv.adu1794, 2025.

Østerhus, S. and Gammelsrød, T.: The Abyss of the Nordic Seas Is Warming, Journal of Climate, 12, 3297–3304, https://doi.org/10.1175/1520-0442(1999)012<3297:TAOTNS>2.0.CO;2, 1999.